Aerodynamic Analysis of a Morphing Wing Using Vorticity Based Solver

by

Shivaranjani Shashank Sathe

A thesis submitted to the Graduate Faculty of
Auburn University
in partial fulfillment of the
requirements for the Degree of
Master of Science

Auburn, Alabama
August 3, 2019

Keywords: vorticity solver, variable camber, unstructured mesh, flexible wing

Approved by

Dr. Roy J. Hartfield, Chair, Professor of Aerospace engineering
Dr. Joseph Majdalani, Professor of Aerospace engineering
Dr. Imon Chakraborty, Assistant Professor of Aerospace engineering

Abstract

This study addresses an efficient approach to analyzing Variable Camber continuous trailing edge flaps (VCCTEF) wings, which mimics the concept of morphing or shape changing wings. The validation model used in this research is a Boeing 757 based Generic Transport Model (GTM) wing semi-span model with 5 sets of flaps at the trailing edge with each set containing three flap elements in the streamwise direction. These three flaps form the trailing section and trailing edge of the airfoil. The geometry containing the fuselage, main wing and 15 three dimensional flaps is modeled in NASA's Open Vehicle Sketch Pad (OpenVSP). The unstructured mesh geometry is then exported from VSP and into FlightStream, a vorticity-based solver, for low speed aerodynamic analysis. The deflection of the flaps is achieved in FlightStream with simple x,y,z rotations coupled with x,y,z translations along user defined and reference co-ordinate systems. The analysis results (C_l, C_d) are validated against wind tunnel data for VCCTEF semi span GTM model. Baseline FLAP0 deflection (with all 15 flaps at zero deflection angle) and some cases with flaps deflected at different angles were available in the wind tunnel data set and were modeled in FlightStream. With a successful validation, a generalized analysis of morphing wings was undertaken as a demonstration of the utility of FlightStream and the underlying surface vorticity approach in conceptual design environments. This approach was shown to capture somewhat nuanced design changes with speed and accuracy.

In summary, the goal of this work was to validate and illustrate the capability of a surface vorticity approaches to model the aerodynamics of morphing wing geometries in the conceptual and preliminary phase of aircraft design.

Acknowledgements

Table of Contents

Table of Figures

List of Tables

Nomenclature

C_l	Coefficient of lift
C_d	Coefficient of Drag
C_{di}	Coefficient of Induced Drag
C_{d0}	Zero Lift Drag Coefficient
α	Angle of attack
VCCTEF	Variable Camber Continuous Trailing Edge Flaps
VSP	Vehicle Sketch Pad
FSM	Flight stream
STL	Stereolithography
L/D	Ratio of Lift to Drag
CFD	Computational fluid dynamics
UTWAL	University of Washington Aeronautics Laboratory
GTM	Generic Transport Model
AASC	Adaptive Aeroelastic Shape Control
MS	Multi Surface

Chapter 1

Introduction

1.1 The Morphing Wing Concept

The first ever successful aircraft built by the Wright brothers and flown on December 17, 1903 used wing warping or morphing wings. The Wright brothers spent untold hours observing birds and how they fly. Birds change the shape of their wings to turn and maneuver, so the Wright brothers used wires and pulleys to control the twist and bend of their wood and canvas wings. Wood and canvas wings performed poorly at high speed, so engineers substituted stiffer materials which required wings with hinged flaps [20]. Today, a century after the first flight of Wright Flyer, the need for energy efficient aircraft has brought back wing morphing as one of several promising technologies for the future of aviation. Though the new morphing wings are inspired by the Wright Flyer, they are far more sophisticated, promising to improve the efficiency, agility and stealth of future aircraft [20].

To facilitate the required actuation loads in an energy and structurally efficient manner, conventional aircraft use mechanical devices composed of rigid components to affect the control. These devices increase the weight of the aircraft and contribute to sub-optimal aerodynamic performance in high lift scenarios. Aircraft shape requirements change according to the flight phase i.e. requirements are different for takeoff, cruise and landing. To meet these requirements, hinged multi-element flaps are deflected at a certain angle. Deflected flaps create a gap between the flap elements and the main wing known as 'slot'. Slot is designed to let high-energy air from lower surface transfer over to the upper surface to reenergize the boundary layer and delay flow separation on the top. The majority of drag penalty due to conventional flap does not come due

to the flaps themselves but due to the large fairings under the wings that house the flap mechanism. This mechanism can result in substantial drag penalty throughout the flight. To overcome this, drag and increase lift, substantial differential power is required, resulting in higher fuel consumption and design defining excess engine mass. Having a more drag is beneficial for flap configuration during landing as it allows the aircraft to maintain a steeper glideslope without speed gain. For takeoff flap setting however, maximizing lift-to-drag ratio is required. The principle of morphing wings is to change the shape of the wing according to flight requirement. This is very challenging mechanically by any means except for activatable smart materials. Approximations to morphed wing shapes can be achieved by fabricating a wing with advanced lightweight composite materials. By eliminating conventional flaps, the overall weight and drag decrease, and lift can increase, making the wing more efficient both aerodynamically, structurally.

1.2 VCCTEF wing

Reducing operational empty weight by using lightweight advanced composite materials is one way to achieve energy efficiency [1] .These materials can provide less structural rigidity while providing sufficient load carrying capacity in a wing application. Aircraft aerodynamic efficiency can decrease significantly with increases in structural flexibility [1]. A NASA study called "Elastically shaped future Air Vehicle Concept" was developed in 2010 to examine a new concept that can enable active control of wing aeroelasticity to achieve drag reduction [1]. This study showed that the highly flexible wing aerodynamic surfaces can be shaped in flight by active control of wing twist and vertical deflection. This controls the local angle of attack on the wing sections which improve aerodynamic efficiency by reducing drag during cruise and improve lift during takeoff and landing.[1]

Aeroelastic wing shaping control can have significant drag reduction benefits. Conventional flaps and slats increase the drag significantly with lift, as a result they are not aerodynamically efficient and are not useful for aeroelastic wing shaping control for drag reduction. A new flap concept called " Variable Camber Continuous Trailing Edge" (VCCTE) was introduced by NASA to achieve this result.[1] Initial study results of this concept proved that there is potential pay-off in drag reduction which would reduce fuel consumption significantly.[1] In order to realize benefits of potential drag reduction by aeroelastic wing shaping control while fulfilling all other performance requirements, the approach for high lift devices should to be considered as a part of the wing shaping control strategy [1]. The critical element of this discussion for the work presented in this thesis is the requirement that the morphed wing shapes must be evaluated for aerodynamic performance in order for the aerodynamic gains to be quantified. Reliable analysis must be completed in a manageable time frame in order for the aerodynamic design of a morphed wing to be driven to an optimum during conceptual design. This requirement provides an opening for reliable, fast-predictor tools such as FlightStream®.

NASA and Boeing are currently conducting a joint study to develop VCCTEF further under AASC within a fixed wing framework. This study built a VCCTEF system for NASA GTM which is based on the Boeing 757 airframe using light weight shape memory alloy technology for actuation and three separate chordwise segments shaped to provide variable camber to the flap. This variable cambered flap is capable of both drag reduction differential lift enhancement as compared to conventional straight, plain flaps.[1]

The semi-span Boeing 757 based GTM model was built and tested at the University of Washington Aeronautics Laboratory (UTWAL). Experimental data from wind tunnel tests is available in reference 1.

1.3 Vorticity Based Solver

The initial aerodynamic analysis of the VCCTEF wind tunnel model was completed using a Vortex lattice Aerodynamic solver, known as VORLAX. VORLAX was one of the first widely used generalized vortex lattice-based solvers and it can accurately approximate the aerodynamic forces and moment coefficients for a wide range of rigid aerodynamic bodies in inviscid subsonic or supersonic flows [2]. The Aerodynamic configuration of the flexible wing VCCTEF model was constructed within the VORLAX by a series of lifting panels that were formed by spanwise and chordwise locations of computing stations specified by user [2]. This vorticity-based solver is only compatible with structured meshes. The main disadvantage of working with structured meshes is the requirement of much higher mesh size on curved surfaces compared to an unstructured mesh [10]. Also, U-V mapping which is used in a structured mesh requires the solver to define four points for each panel even if one side of the quadrilateral has been collapsed to a triangular panel which results in unnecessary use of memory when defining the geometry [10]. The advantage of a structured mesh is its ability to refine certain areas of the mesh easily. Individual panels can be refined or deleted to increase mesh fidelity. However due to the requirement to define panel edges as bound or trailing vortices during the calculation of induced loads on local panels, vorticity-based solver are unable to use unstructured meshes with arbitrary panel orientation [10]. This is a significant limitation for modern engineering workflows involving CAD, unstructured mesh generators, and conventional CFD compatibility.

In 2013, FlightStream® was developed in part to overcome the unstructured mesh challenge for vorticity-based solutions. FlightStream uses an application of vortex rings on a triangular panel.[10] FlightStream has since evolved into a modern engineering tool capable of CAD import, onboard state-of -the-art meshing, analysis of viscous effects in high lift scenarios, scripting for workflow integration, and advanced post processing. FlightStream® has been validated for a wide range of conventional and contemporary air vehicle configurations but not for morphing wings [23]. The goal of the present research is to validate FlightStream® using the aerodynamic performance of the VCCTEF flexible wing model in and to then apply FlightStream® to a practical morphing wing aerodynamic analysis problem.

The flexible wing wind tunnel model tested in UTWAL facility is closely replicated in NASA's OpenVSP software. The unstructured mesh is created in VSP using COMPGEOM and then exported to FlightStream as STL file. Elements of the geometry used in the wind tunnel test is regarded as proprietary and some critical geometric parameters are omitted from Ref. 1 (Nguyan), therefore, no representation is made in this work regarding the shape of the proprietary wind tunnel geometry. The geometric definitions provided in this work are provided to describe the outer mold line used in the analysis only.

1.4 Thesis Overview

This thesis will validate FlightStream for its application to analyze VCCTEF Flexible wing. Chapter 2 will cover the detailed explanation of creating a geometry in OpenVSP followed by its setup in FlightStream® in chapter 3. Chapter 3 will also cover elements of FlightStream® required for this analysis. Chapter 4 describes the validation results against wind tunnel data of Flexible VCCTEF wing for twelve different flap deflection cases. Chapter 5 describes the design and analysis of a more refined morphing wing with sample results. The concluding chapter of

the thesis summarizes the success of the analysis undertaken and describes future work possibilities .

Chapter 2

Design And construction of a Flexible wing VCCTEF Geometry in OpenVSP

2.1 Baseline model:

The baseline model used for this analysis is 5.5% scaled research transport platform called the Generic Transport model (GTM). This geometry represents a single aisle 200 passenger capacity transport aircraft generically approximating a Boeing-757. GTM has been tested in NASA Langley Research center's 14-feet by 22-feet wind tunnel. Due to availability of its wind tunnel data, this model was chosen for VCCTEF system analysis in reference 1.

2.2 Wind Tunnel Model:

For exploratory assessment of the aerodynamic potential of the VCCTEF concept, a 10%-scaled aeroelastic model of a softened Boeing 757-based GTM wing was constructed for a wind tunnel experimental investigation in the University of Washington Aeronautical Laboratory (UWAL). The semi-span of the model is 73.29 inches. The model has 5 sections of VCCTEF attached to outer wing. Each section has three cambered flap segments that can be controlled individually. Each of these cambered flaps are connected to the adjacent section by a flexible and supported material installed with the same shape and camber, thus providing continuous flaps throughout the wingspan. To improve aerodynamic performance, VCCTEF relies on two mechanisms: wing twist optimization for flexible wing design and variable camber and continuous trailing edge for improved aerodynamics. This fixed wing technology may be referred to as Performance Adaptive Aeroelastic Wing (PAAW). For the wind tunnel model,

VCCTEF parts were fabricated using 3D printing. Flap segments are mechanically interlocking aerodynamic surfaces in the chordwise direction. The flap segments were hinged at three chordwise locations and were designed to be fully adjustable. The detailed dimensions of the wind tunnel model are shown in figure 1 and 2.[1,3]
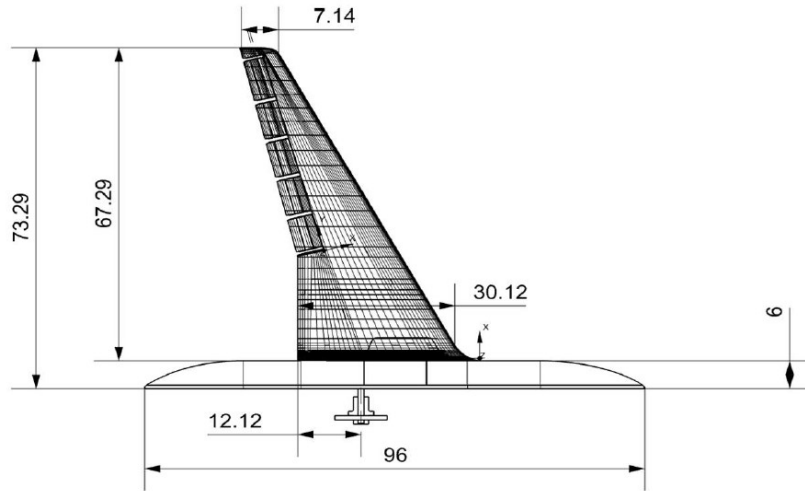
Figure 1: Dimensions of Wind tunnel Model (measurements in inches)[1,3]
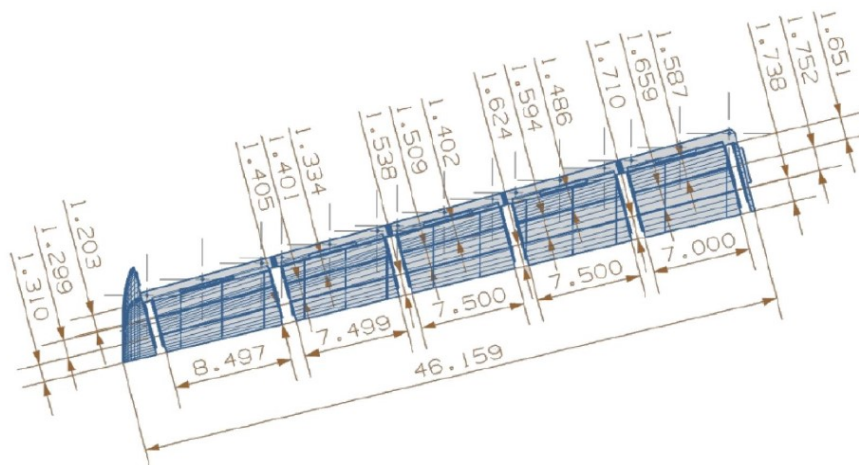
Figure 2: Detailed dimensions of VCCTEF Flap sections (measurements in inches)[1,3]

The objective of wind tunnel tests was to prove the benefits of VCCTEF design as a drag reduction control device and the ability to simulate the aerodynamic performance at relatively low-cost. The model scaling parameters are shown in table 1 [1].

	Full-Scale	Semi-Span Model
M_∞	0.797	0.1162
C_L	0.51	0.51
h, ft	36,000	0
q_∞, psf	211.09	20.00
$S/2$, ft^2	975.5	9.638
$\bar{c}$, ft	16.6417	1.5963
$b/2$, ft	62.4167	6.1262

Table1: Model parameters [1,3]

The semi span with half fuselage model was tested in the wind tunnel.

2.3 Replicating Geometry in OpenVSP:

The main components of the wind tunnel geometry are modeled in OpenVSP (VSP). VSP is an open-source tool designed for the purposes of rapidly generating 3D aircraft models in the early conceptual phase of aircraft design. VSP allows user to divide each component into different sections which makes obtaining desired shape easy. All the aircraft parts are placed relative to each other in VSP. For the required wind tunnel model, the fuselage, main wing section and fifteen flaps are modeled in VSP and placed relative to each other. The required

rotation of the flaps and the filling of gaps was performed in FlightStream® as described in Chapter 3.

2.3.1   Fuselage:

In VSP under the main menu tab and model, selecting a geometry tab opens a geometry Browser (Figure 3). In the geometry browser, selecting Fuselage and adding the component creates default fuselage geometry in workspace. Selecting Fuselage option displayed in Geometry browser opens another window named 'Fuselage' (figure 4) which allows its modification using x,y,z translation and rotation under XForm tab, specifying length under DESIGN tab, and modifying cross section under XSEC tab. For this geometry, the fuselage is divided into eight sections. The half fuselage geometry (along the length) in wind tunnel model is mainly used as a support for the wing with maximum radius of 6 inches. In VSP model, Sections 0 and 7 of the fuselage are point type, while sections 1 through 6 are circle type with 12-inch diameters. The specified length of the fuselage is 96 inches.
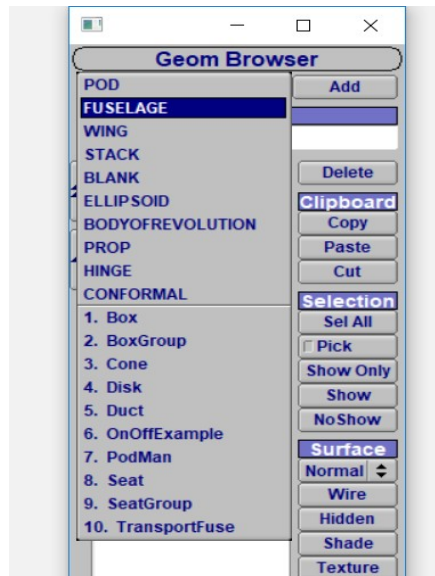
Figure 3: Geom Browser
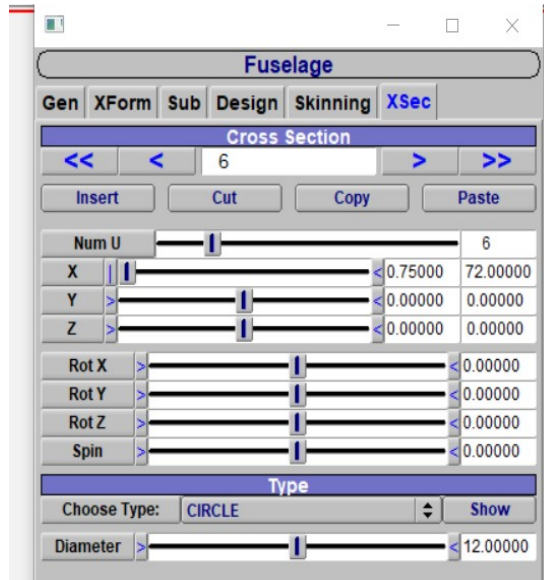
Figure 4: Fuselage modification window

2.3.2 Main Wing and Airfoil:

The wind tunnel model approximates a Boeing 757 wing. The coordinates for the Boeing 757 airfoil are not disclosed. For this work, a grid generation closely replicating a Boeing 757 airfoil was obtained from reference 19 as shown in Figure 5. The coordinates were extracted manually from this figure using Autodesk Inventor. The picture of the airfoil was imported in Inventor and, using the Spline command the shape of the airfoil was traced carefully.   The Point command was then used to extract the x,y location of each point. VSP uses its own file format for airfoil points.[13]. The first line is a file format identifying header which must contain "AIRFOIL FILE" to be useful for VSP. The second line is the airfoil name which will be displayed in VSP. The third line is a flag to indicate a symmetrical airfoil. The fourth and fifth lines specify the number of points which define the upper and lower surfaces. Surfaces are given as a series of (x,y) pairs for the top surface first, then for the bottom surface. Points are specified

from leading edge to trailing edge and there is a blank line between two sets of points. The leading edge will be at (0,0) and trailing edge will be at (0,1) for most cases but not always.[13] The AF file used for this model is given in Appendix A.
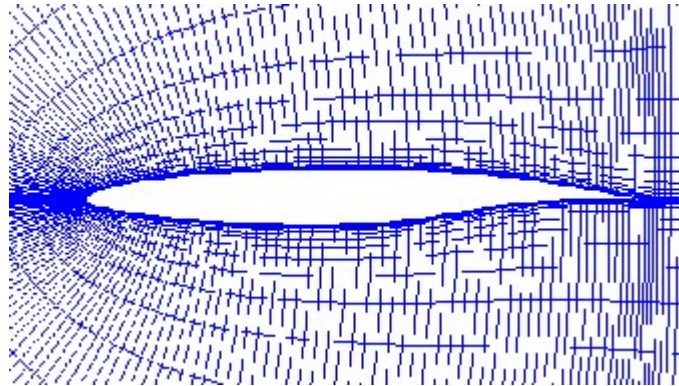
Figure 5: Airfoil used in VSP model [19]

The default wing geometry was created in the same fashion as Fuselage using the geometry browser. VSP creates the full span wing by default along the XZ symmetry plane. Since the wind tunnel model is a semi-span model, the symmetry along the XZ plane was verified. The wing modification window in VSP allows the user to specify span, and root chord incidence angle under PLAN tab. The division of wing, specifying root and tip chord as well as sweep and twist are specified under the SECT tab. Importing the AF file is completed under the AIRFOIL tab and then the airfoil modifications are completed under the BLENDING and MODIFY tabs. The wingspan of the wind tunnel model is 67.29 inches, root chord is 30.12 inches and tip chord is 7.14 inches. The mean chord length of the wing is 19.155 inches and wing is swept back from the mean chord at 27 degrees. The wing is divided into 12 sections. These sections are very useful to trim the upper part of the main wing and create exact space

needed to fit the flaps. The trailing edges of the airfoils in section 4 to 10 were trimmed along the relative chord length. The best way to get an accurate trimmed wing is to use a simple continuous wing of same dimensions as a reference. Aligning trailing edges of all the flaps with the trailing edge of the main wing and then trim the trailing edge of the main wing until it matches with the leading edge of the flaps attached directly to the main wing. The AF file can be imported into VSP under the AIRFOIL tab. Select the type of airfoil as AF_FILE, and then select the required file from proper location.

The aeroelastic deflections of a flexible swept back wind tunnel model contribute significantly to the aerodynamic performance due to wash out effect resulting from wing bending and twist.[1] This suggests that the main wing has some pre twist (apart from twist generated due to flap deflections). Since the information about the twist on Boeing 757 airfoil is not available the closest information found was related to the Boeing 737. The root chord for Boeing 737 is at 4-degree twist and tip chord is at zero. Therefore, these values are used in VSP model. Since the VSP model is divided into 12 sections and last three sections i.e. 10, 11 and 12 contributes to the tip of the VCCTEF wing, airfoils 10,11 and 12 are at zero angle. Airfoil 0 (root airfoil) is at 4-degree angle and airfoil sections between 0 to 10 are at a 0.4-degree lower angle with respect to its previous airfoil section. Figure 6 shows the geometry of the fuselage and the main wing obtained after modifications.
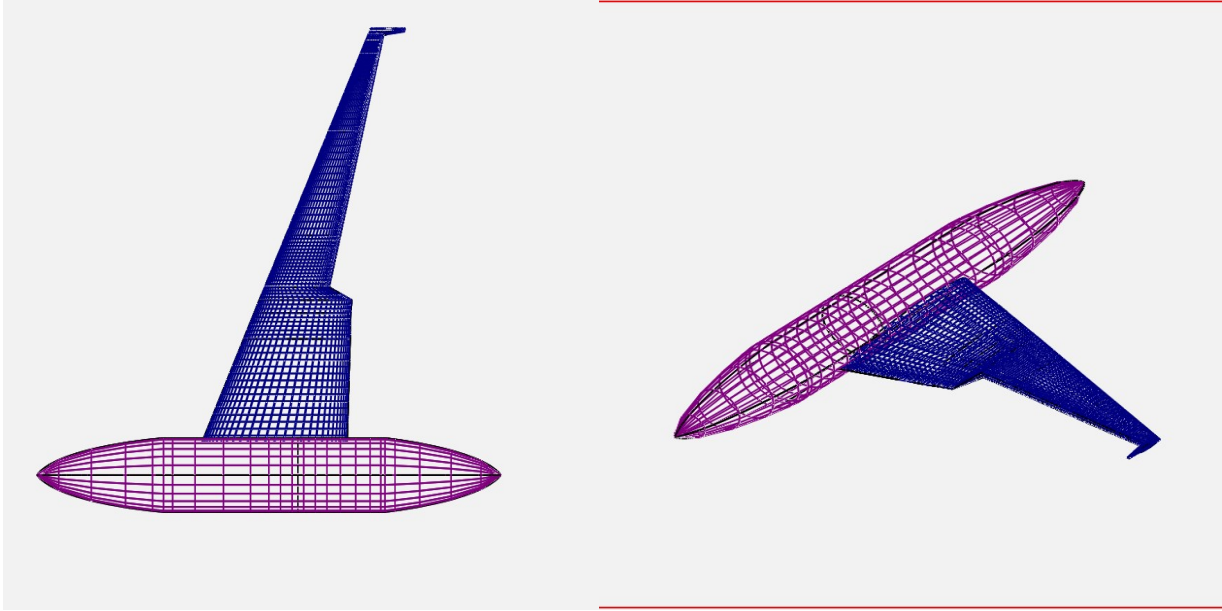
Figure 6: a) Top view of main wing and fuselage   b) ISO view of main wing and Fuselage

2.3.3   Flaps:

There are 15 different flaps in this geometry with dimension given in figure 2. In VSP, each flap is made of individual 3D wing component. The process of modelling all the flaps is similar so in this section, modelling of only one flap is explained in detail.

Referring to Figure 2 and considering the first flap directly connected to the main wing, the flap is 7 inches long with one side adjacent to the lower part of the main wing is 1.651 inches wide and the other 1.587 inches. First step was adding a wing component into the workspace and switching off the XZ symmetry. Modifying that wing to 7 inches span, 1.651 root chord, 1.587 tip chord, zero sweep and importing the correct AF file for both airfoil sections created a flap which was used as a reference. Translating and rotating this flap along x,y,z axis as needed to

place it right behind the main wing and in between the space created for flaps. In VCCTEF system, shape of three flaps joined together and at zero deflection angle contributes to the last section of the airfoil (Fig 8). To get each flap's airfoil section as accurate as possible, another wing was added to the workspace. Modifying it to 7 inches span, setting root chord and tip chord values same as the root and tip chord values of the main wing's section correspond to the position of first flap and trimming the leading edge and trailing edge along the chord length of this wing until it matched the leading edge and trailing edge of the reference flap and setting sweep angle to zero created the required airfoil section of the first flap. Following a similar method of chord length trimming for the second section of the airfoil of the same wing generated the second airfoil section completing the required model of first flap. A similar procedure was followed for creating rest of the flaps only with dimension changes. Trimming the wings for modelling flap sections created a small gap between two flaps (Fig 7). This Problem was fixed in FlightStream® by patching up all the flaps. Also, the distance between each flap set is 1 inch, which was also corrected in FlightStream® since measuring accurate distance was easier in FlightStream as compared to VSP. Figure 8 shows the complete model of VCCTEF flexible wing with all fifteen flaps.
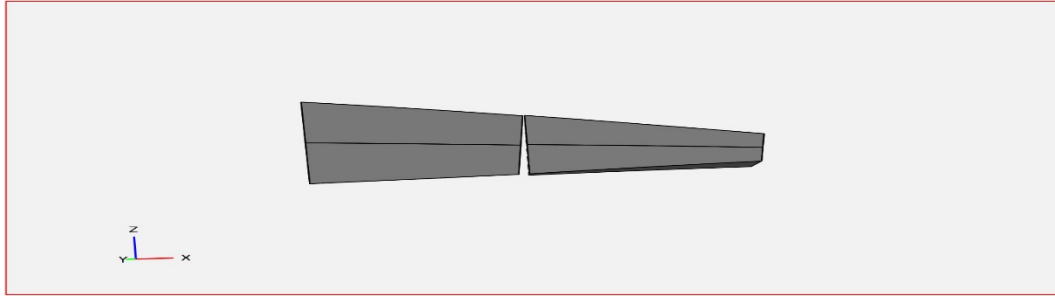
Figure 7: Gap between two flaps in VSP model
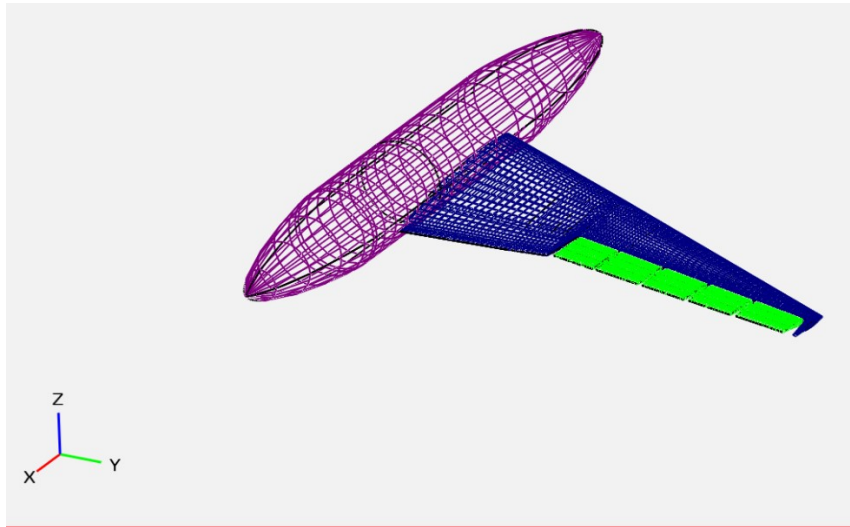
Figure 8: ISO view of VCCTEF flexible wing VSP model
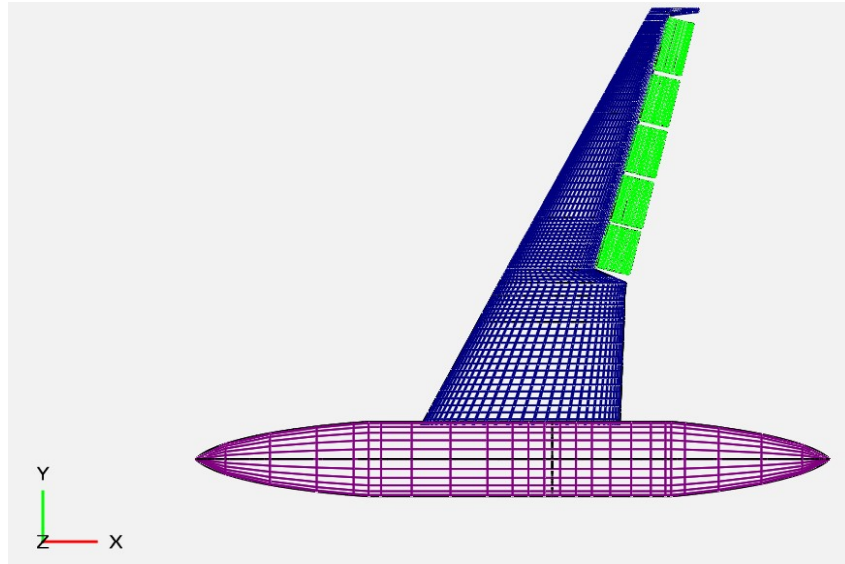
Figure 9: Top view of VCCTEF flexible wing VSP model

2.4 Generating Unstructured mesh and exporting the model:

The triangulated wireframe is created by connecting the diagonals of the quadrilateral wireframe. (Figure 8 a and b shows model with quadrilateral wireframe)[17]. The resolution of the triangulated wireframe is determined by the resolution of the quadrilateral wireframe. [17] Airfoil points were refined in wing geometry's window, under GEN tab and tessellation option, Num_W specified for main wing are 57. The spanwise wireframe was refined under SECT tab and 'Num interpolated Xsecs'. The spanwise wireframe was refined section by section. Similar quadrilateral refinement was done for all the flaps. After quad refinement, under Analysis tab in the main menu, Comp Geom option was selected. It opened a Comp Geom window where selecting 'execute' created unstructured mesh on the VCCTEF flexible wing VSP model. The unstructured mesh generated by OpenVSP is shown in figure 10.

17
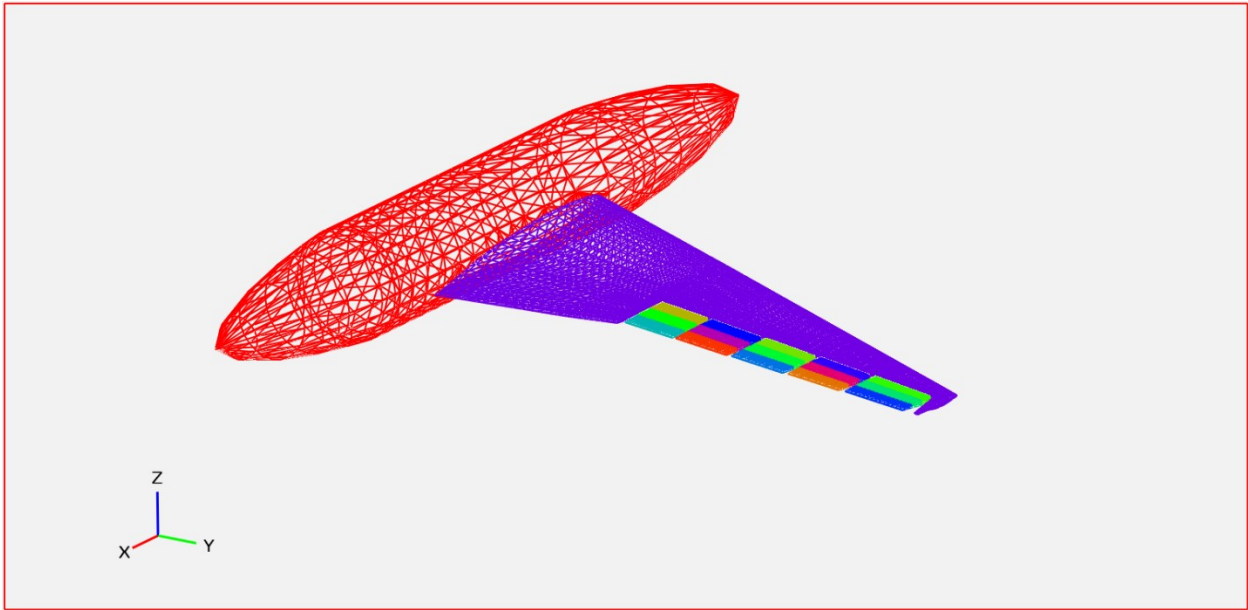
Figure 10: Unstructured mesh Generated by VSP after Comp Geom (ISO view)
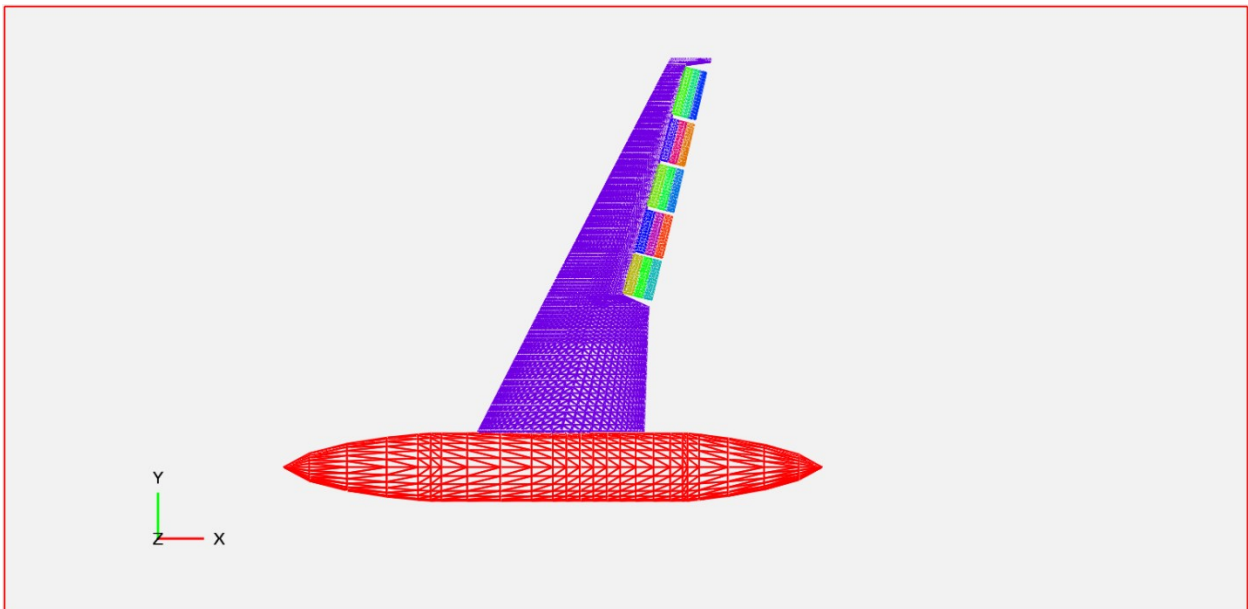
Figure 11: Unstructured mesh generated by OpenVSP after Comp Geom (Top view)

VSP has capability to export models in various file formats compatible with aerodynamics analysis programs including 3D systems stereolithography (STL) files used by FlightStream. STL files can be generated in either high quality mesh grid or simple lower quality mesh grid. Lower quality grids seem to work well and yield good results when loads are calculated using vorticity so that option was used for generating STL files for FlightStream® except in cases where viscous effects were considered. Modeling viscous effects in FlightStream® requires a more accurate pressure distribution, which in turn is more dependent on a refined grid in areas of high-pressure gradients such as leading edges of wings.[9]

Chapter 3

FlightStream Setup and Analysis

3.1 Brief Overview of FlightStream:

The FlightStream® solver is a vorticity-based flow solver developed by Dr. Vivek Ahuja beginning in 2013 as an efficient alternative to typical CFD solvers [9]. FlightStream® has the ability to model compressible and incompressible flow solutions below Mach number of approximately 0.8. FlightStream calculates induced lift and drag using the Kutta-Joukowski theorem and skin friction drag from the local vorticity distribution [9]. For modeling viscous effects, the wing pressure distributions are used, requiring higher quality surface meshes. Unlike volume-based solvers, FlightStream® can generate solutions using unstructured surface meshes by using an application of vortex rings on multisided panels [9]. This reduces the amount of time and effort required to create a mesh suitable for FlightStream® use. Within the solver, vortex filaments are placed on the perimeter of each facet of the mesh to form vortex loops. By applying the Biot-Savart law, it is possible to determine induced velocity on a point in space from the segment of the vortex loop located on one of the edges of a panel due to that vortex filament [10]. This same evaluation can be done for the other two sides of triangular facet to determine the total induced velocity at a point in space from the entire vortex loop located on the panel [10]. The vorticity strength can be found by applying the Von Neumann boundary condition at control points on the sub panel surface element. After vorticity strengths are determined, such that the Von Neumann condition is satisfied on every panel on the surface of the vehicle, the induced velocity at any point in space due to the presence of the vehicle in a stream can be found [10].

Instead of using a structured wake sheet, which was the case with many legacy vorticity-based solvers, FlightStream® optionally uses a relaxed wake strand model. After trailing edges are marked either manually or automatically in the solver, FlightStream® creates wake strands by analyzing contributing panel edges and determining whether they have additive or diminishing effects on the vorticity strengths of the wake strands. The contributing panel edge classifications are decided by the panel's orientation relative to the node. The net vorticity of the geometry is propagated downstream by the wake strands with the only decrease to vorticity strengths due to viscous effects. FlightStream numerically propagates wake strands downstream with varying vorticity to simulate viscous effects in the wake. The size of pseudo-time steps used for the numerical propagation along each individual step of a wake strand segment is selectable. This allows the solver to change the local step size based on flow conditions while still propagating all wake strands to a user designated Trefftz plane. The flexibility of the relaxed wake strand model allows FlightStream to more accurately describe the propagation of filaments downstream from lifting surfaces which makes it possible to capture the interaction between different segments of geometry.[10]

Most of the legacy vorticity-based solvers apply the Kutta-Joukowski theorem to calculate lift based on vortex strength and flow conditions. But, due to arbitrary orientation of panels in unstructured surface mesh, this is not possible. FlightStream® solved this problem using a method to calculate shed vorticity in which panel orientation is irrelevant [10]. A more detailed description of the physics employed by FlightStream® are given in Reference 5.

3.2 VCCTEF Flexible wing setup in FlightStream

The STL file created in OpenVSP was imported in FlightStream®. FlightStream® uses default units as meters. Since dimensions used in VSP were in inches, while importing STL file in FlightStream it is important to change dimension from meters to inches. FlightStream automatically converts inches to its corresponding meters values after importing the model. The inviscid effects are essentially unit independent; however, accurate modeling of the viscous effects such as skin friction and boundary layer separation are directly dependent on correct dimensions being used.

After importing the geometry first step for solving is to establish the corrected geometric settings by translating the flaps in the "Y" direction so that there is exactly a 1-inch gap between the Flaps. Individual surfaces can be selected under simulation tab and geometry option. In the wind tunnel experiment, the C_l and C_d were calculated for 12 different VCCTEF deflection cases which are specified in Table2. The first case serves as a baseline which is FLAP0 in which all 15 faps are at zero deflection angle.

Table2: VCCTEF deflections (all measurements are in degree) [1,3]

FLAP	Section1	Section2	Section3	Section4	Section5
FLAP1	(5/ 4/ 9)	(6/ 7/ 9)	(9/ 7/ 10)	(7/ 8/ 10)	(6/ 9/ 9)
FLAP2	(3/ 2/ 10)	(4/ 5/ 4)	(5/ 3/ 4)	(4/ 6/ 5)	(5/ 10/ 10)
FLAP3	(2/ 3/ 5)	(5/ 6/ 5)	(6/ 6/ 11)	(5/ 6/ 5)	(4/ 6/ 5)
FLAP4	(2/ 5/ 9)	(3/ 6/ 3)	(4/ 1/ 6)	(2/ 5/ 2)	(0/ 0/ 0)
FLAP5	(0/ 0/ 0)	(2/ 5/ 1)	(4/ 2/ 7)	(3/ 5/ 6)	(3/ 8/ 9)
FLAP6	(1/ 1/ 1)	(0/ 2/ 0)	(0/ 0/ 2)	(0/ 0/ 0.5)	(0/ 0/ 0)

FLAP7	(3/ 3/ 4)	(2/ 3/ 2)	(0/ 0/ 3)	(0/ 0/ 0)	(0/ 0/ -2)
FLAP8	(4/ 0/ 0)	(4/ 0/ 0)	(5/ 0/ 0)	(5/ 0/ 0)	(4/ 0/ 0)
FLAP9	(0/ 0/ 6)	(0/ 0/ 6)	(0/ 0/ 8)	(0/ 0/ 6)	(0/ 0/ 6)
FLAP10	(2/ 3/ 2)	(3/ 3/ 1)	(4/ 2/ 5)	(2/ 5/ 2)	(2/ 5/ 3)
FLAP11	(-1/ 0/ -3)	(0/ 0/ -6)	(-1/ -4/ 0)	(-2/ 0/ -5)	(-4/ 0/ -4)

In Table 2, the convention given in Figure 12 is used. A flap section is a portion of VCCTEF along the spanwise direction. There are 5 flap sections numbered from 1 inboard to 5 outboards. Each Flap section is comprised of three camber segments which are labelled as 'A' for innermost segment, 'B' for middle segment and 'C' for trailing edge camber segment. The position angle in table 2 are denoted by (A/B/C) where A,B,C are flap positions in degrees relative to the forward flap segment. For flap 'A', position angle is with respect to the fixed wing portion.[1,3]
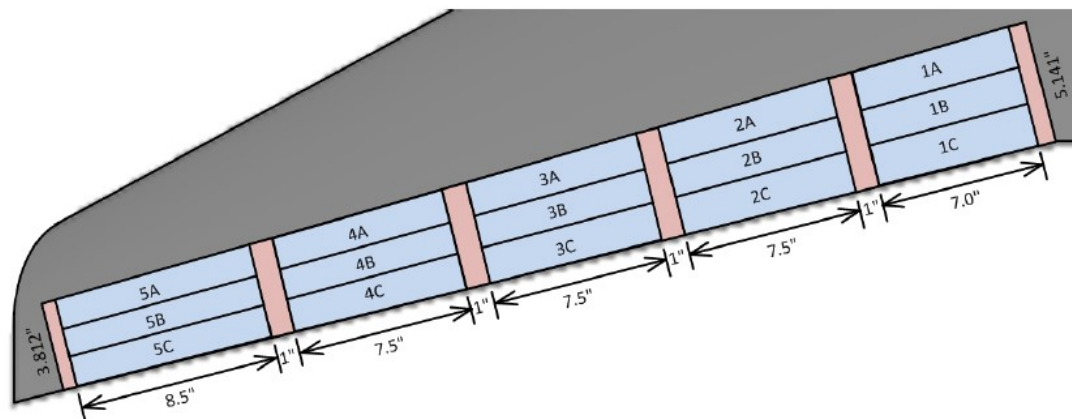

Figure 12: VCCTEF flap notations [1,3]

These deflections were achieved in FlightStream by specifying a User co-ordinate system for each flap and rotating the flap along the "Y" axis at a specified deflection angle then using X and Z rotations and X,Y,Z translations to bring the Flap to its required position i.e. leading edge of the Flaps are aligned with trailing edge of the previous flap. For flap 'a', its leading edge should match with the trailing edge portion of the fixed wing. The FLAP0 case does not require the use of user defined co-ordinate systems as all the flaps are at zero-degree angle.

Flaps modeled in VSP are individual 3D components. Since Flaps in the VCCTEF system have continuous camber, it is important to connect all these flaps to each other. This was done in FlightStream manually using mesh repair. The faces between all the flaps were deleted by using the face selection option and then selecting delete as shown in Figure 13. The process was repeated for each flap section. After deleting all the faces, next step was to connect flap surfaces to each other.
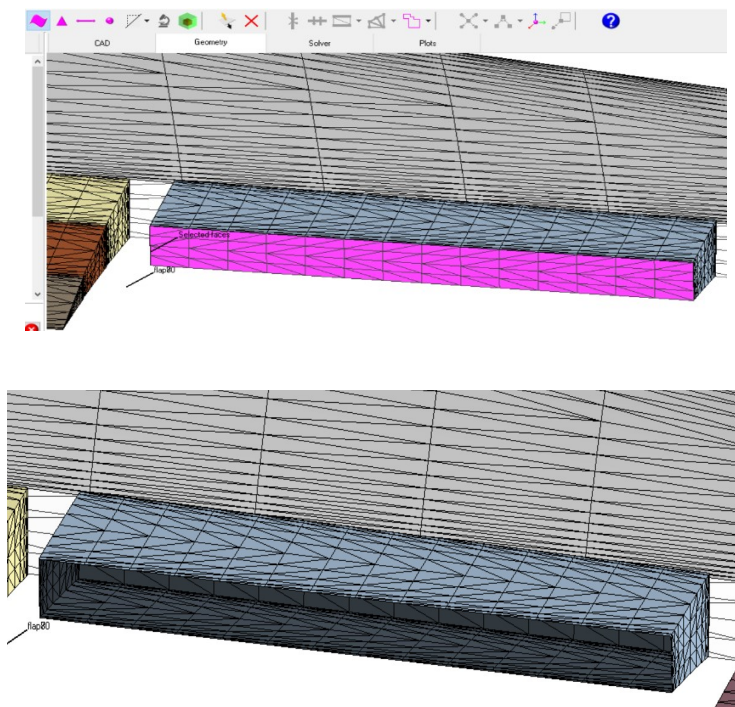

Figure 13: Before and after deleting face between flaps

Since unstructured mesh on the all the flaps were similar, it was easy to connect vertices to each other by selecting two vertices at a time and then using 'merge vertices' option in the FlightStream® toolbar. After merging all the flaps to each other (section wise) all the 5 flap sections were connected to each other to form a continuous trailing edge. Figure 14 shows the cross section of the connected flap section and figure 15 shows all the flap sections forming continuous trailing edge.
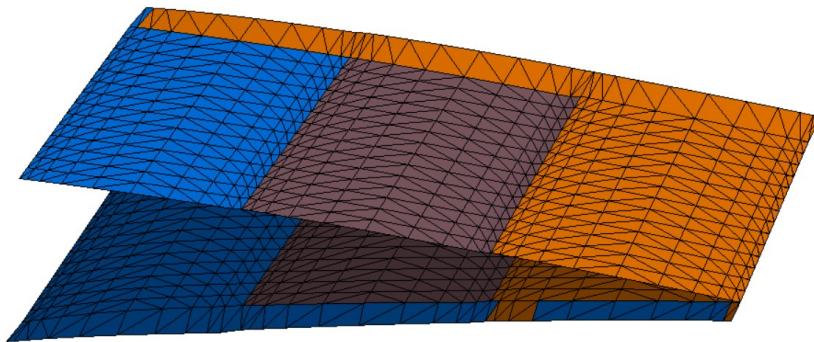

**Figure 14: Cross section of one flap section after mesh repair**
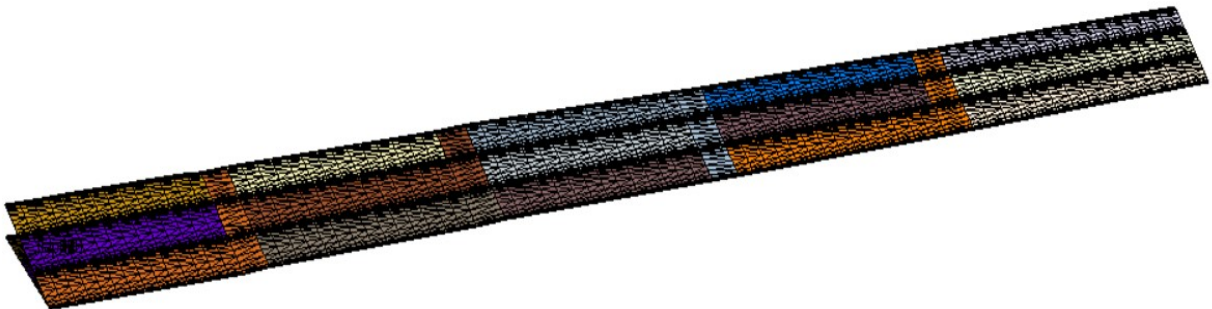
Figure 15: All flap sections connected to each other forming Continuous trailing edge

The last step before initializing a solver was to connect these flap sections to the fixed wing part. Like flaps, fixed wing's back face was deleted where flaps are positioned. Using edge selection tool, corresponding edges of the fixed wing and adjacent flap were merged. Similarly, Section1 and Section 5 of the flaps was connected to the side and tip of the fixed wing respectively. The final model for FLAP0 after all the mesh repair is shown in Figure 16. Trailing edges were selected manually. Flaps 1c, 2c, 3c, 4c, 5c and the main wing or fixed wing were marked for trailing edges and wake termination nodes was detected automatically by FlightStream®. Figure 16 shows trailing edges highlighted in green and wake termination node marked with green dot.
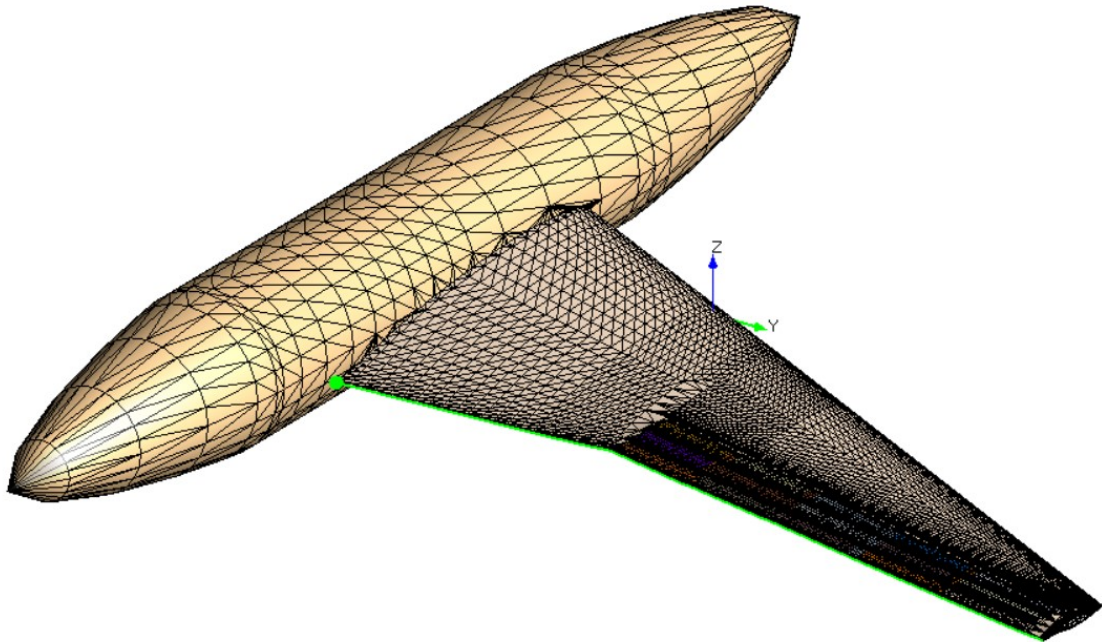

Figure 16: All flap sections connected to each other forming Continuous trailing edge
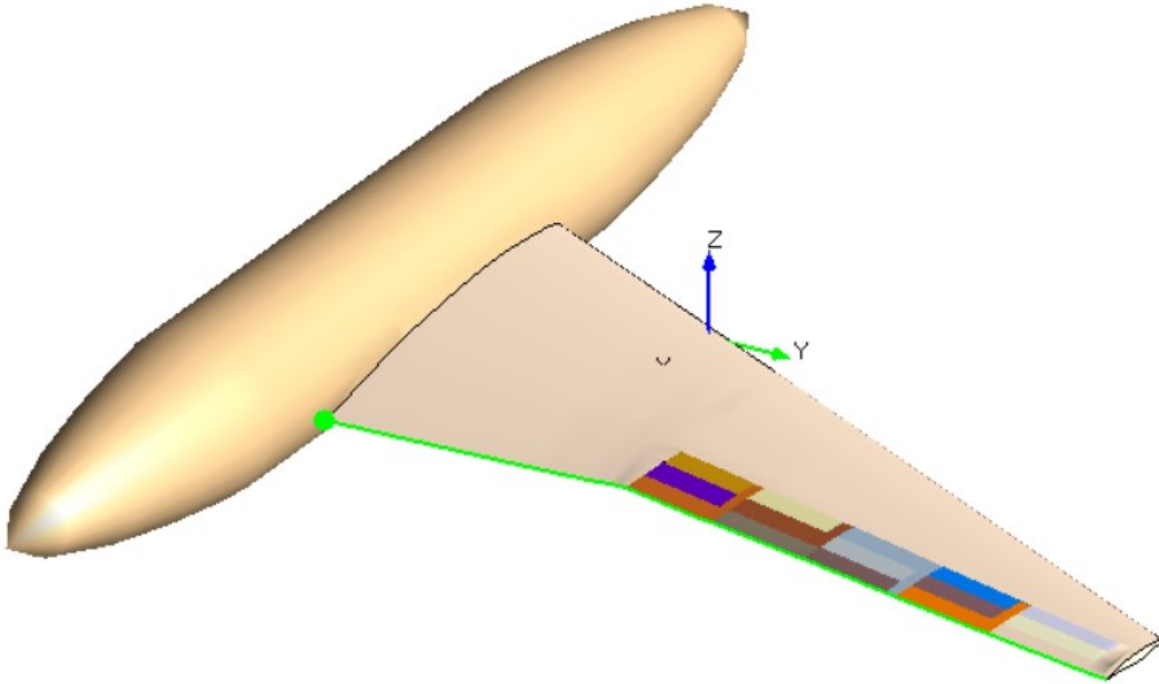
Figure 17: Final VCCTEF FLAP0 model after mesh repair

After marking trailing edges and wake termination node, the solver was initialized. Mathematically, this is equivalent to setting up the "A" matrix in classic vortex solution theory [22]. As with the wind tunnel test, aerodynamic forces and moments were analyzed at a nominal Mach number of 0.1162 (i.e. freestream velocity of 39.54 m/s at sea level conditions) with a reference area of 0.89m^2. The solution was collected for nominal angles of attack ranging from 0 to 6 degrees with respect to root chord inclination. Although the compressibility effects are expected to be quite small, the model was setup to be compressible and the Prandtl-Glauert compressibility model was used for analysis. The FlightStream® solver normalizes the aerodynamic forces and moments by using the user-specified reference length (L_{ref}), reference velocity (V_{ref}) and reference area (S_{ref}) using the following equations: [18]

$$Cl = \frac{L}{Q * S_{ref}^2}$$

$$Q = 0.5 * \rho * V_{ref}^2$$

$$C_{di} = \frac{D_i}{Q * S_{ref}}$$

$$C_{d0} = \frac{D_0}{Q * S_{ref}}$$

The validation of the FlightStream® results against wind tunnel data is presented in the Chapter 4 for all deflection cases. As with the FLAP0 case, mesh repair was completed for all other deflection models before initializing the solver. As an aside, it is understood by the author that a more streamlined approach for deforming the mesh is currently available in FlightStream®.

Chapter 4

FlightStream Validation results

The aerodynamic force and moment data was obtained during α-sweep runs to match the cases for which experimental data is available in Ref. 1. C_l and C_d values obtained by FlightStream® analysis are validated against C_l and C_d data presented in the Wind tunnel VCCTEF Flexible wing experiment. The design lift coefficient for the wind tunnel model is 0.51. To fully validate the loads, approximate C_d values at lift coefficient value of 0.51 are also compared for all the cases. To calculate inviscid loads, the vorticity model in FlightStream® is used for lift and induced drag and the Reynolds number-based model is used for skin friction. A pressure-based loads model is available in FlightStream®; however, more refined meshes are required to accurately capture the pressure distribution that is required to capture the shed vorticity and the resulting lift and drag from the Kutta-Joukowski Theorem. The finer meshes and associated pressure-based loads are used in high lift scenarios in which flow separation is likely to occur.

4.1 VCCTEF deflection results:

4.1.1   FLAP0 configuration results:

Figure 18 shows vorticity distribution on the FLAP0 model. Its detailed configuration, wind tunnel settings and mesh repair is described in detail in chapter 3.
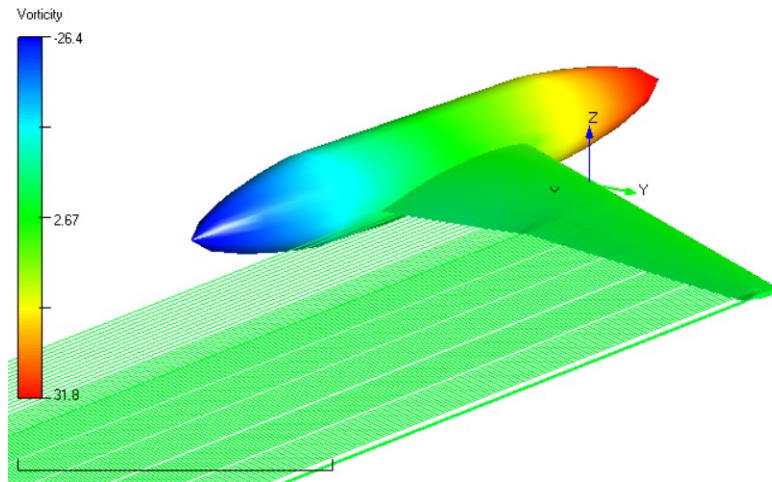
**Figure 18: Vorticity distribution on FLAP0 VCCTEF Flexible wing model**
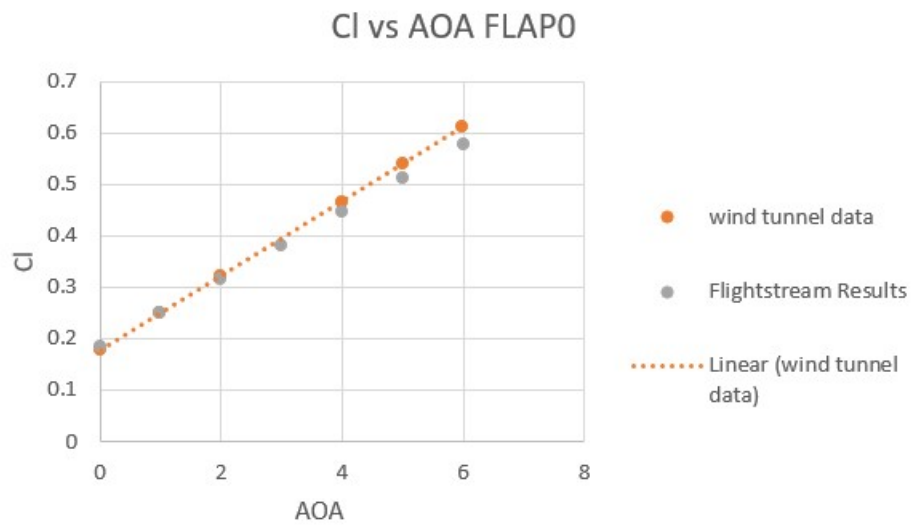
**Figure 19: Lift curve comparison for FLAP0**
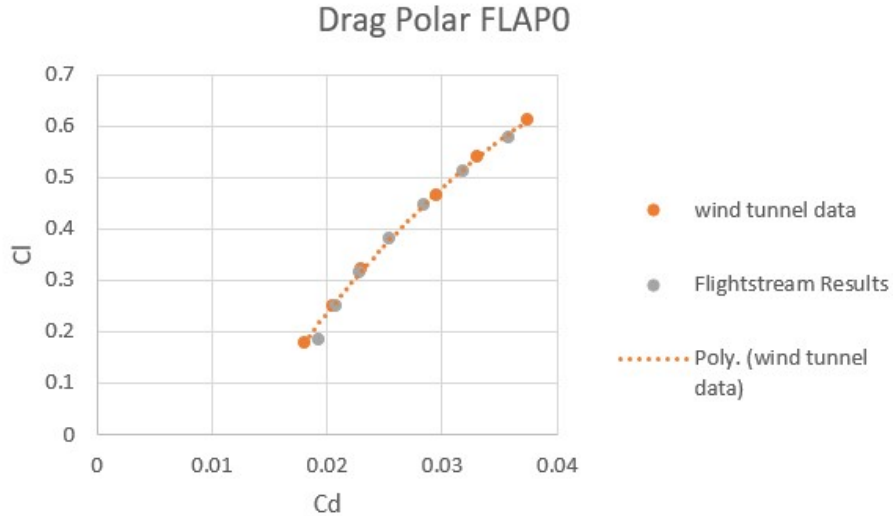
Figure 20: Drag Polar comparison for FLAP0

As seen in Figure 19 and Figure 20, The FLAP0 model tested in FlightStream® proved to be in good agreement with wind tunnel data but the results diverge slightly from the wind tunnel data decreases with increasing in angle of attack. The drag coefficient at the ideal C_l of 0.51 for wind tunnel model is 0.0317 while value obtained through FlightStream® analysis is 0.0319 giving out percent error of 0.63. This drag value is considered as 0 count and used as reference value to compare drag reduction in following VCCTEF cases.

4.1.2 FLAP 1 Configuration Results:

In this configuration, all the flaps are at full deflection. The total deflection of the flap from inboard to outboard flap sections respectively is, 18°, 22°, 26°, 25°, 24°. This is the model with the highest deflection angles compared to all other configurations. Figure 21 shows the

FlightStream model after deflecting the flaps at their respective angles as shown in table 2. Figure 22 shows vorticity distribution or distributed circulation on the model.
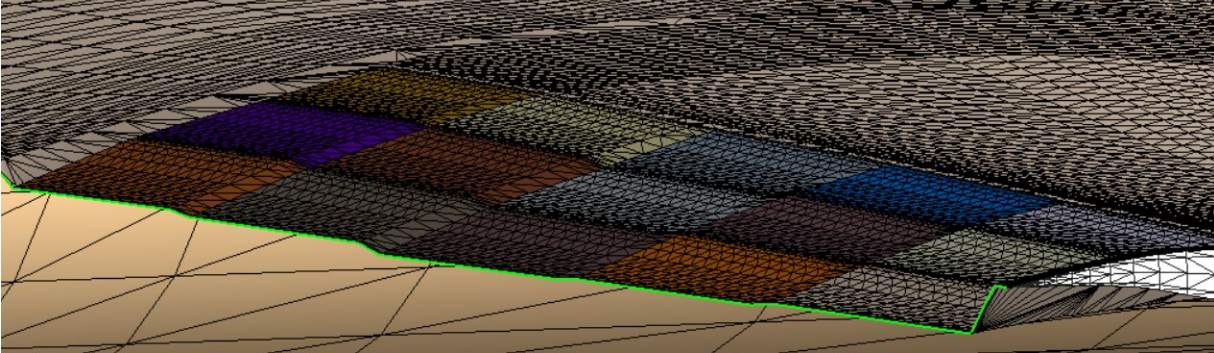

Figure 21: VCCTEF FLAP1 deflections
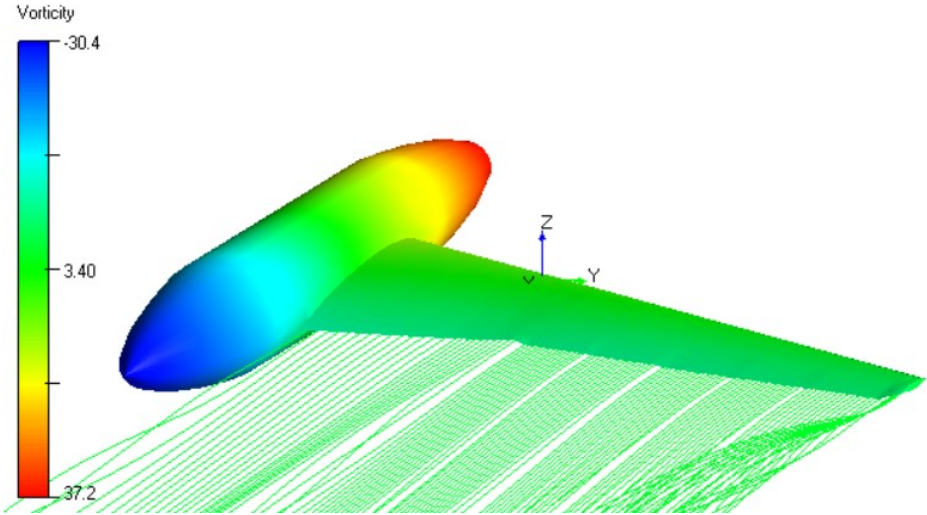
**Figure 22: Vorticity distribution on FLAP1 configuration**
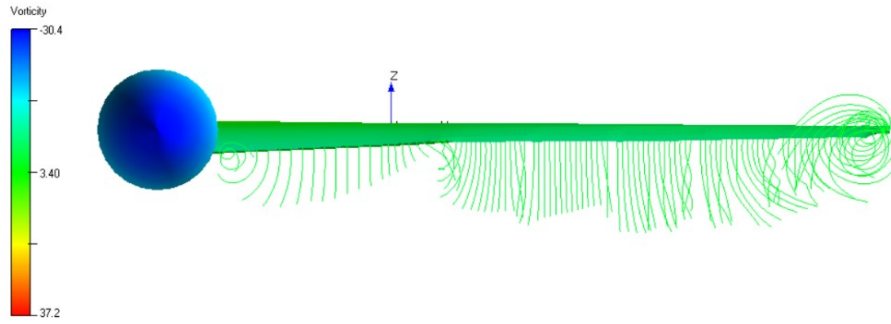
**Figure 23: Vortex shedding for FLAP1 configuration**
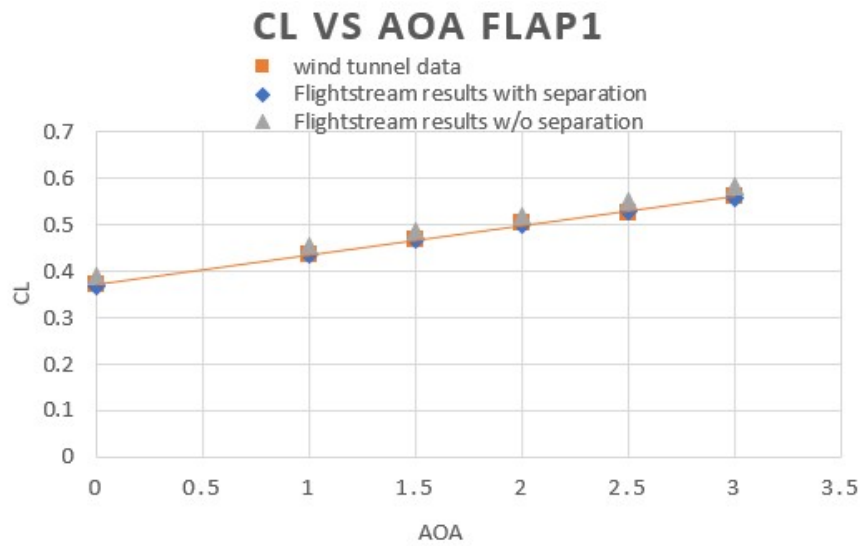
**Figure 24: Lift curve comparison for FLAP1**
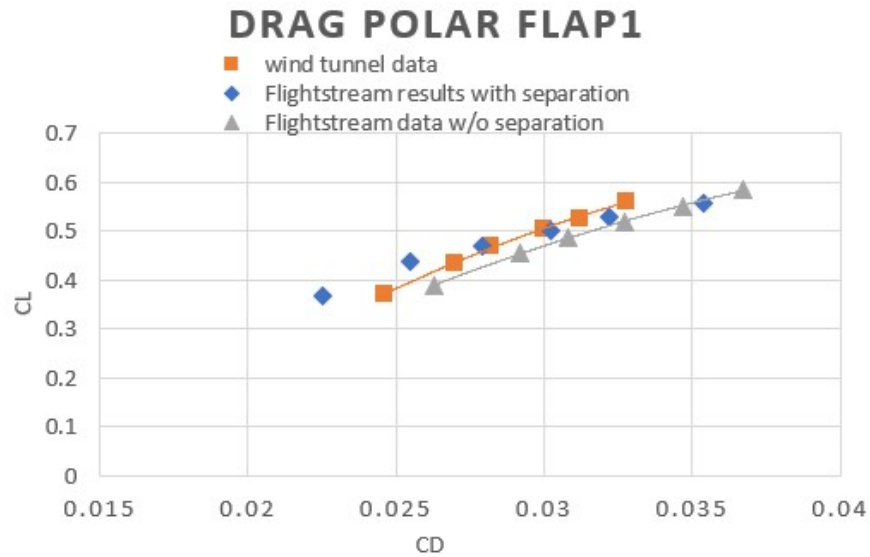
Figure 25: Drag Polar comparison for FLAP1

FLAP1 configuration analysis was completed in FlightStream using two different loads and moments model, vorticity and pressure model with enabled turbulent transition and flow separation. Figure 24 and 25 shows solution obtained using both models and its comparison with wind tunnel data. FlightStream overpredicted lift coefficients for vorticity model and slightly underpredicted for pressure model with flow separation. But overall lift curve agrees well with wind tunnel data for both FlightStream model solutions. On the other hand, drag generation is more on the FlightStream model for vorticity solution compared to wind tunnel model. Drag coefficient at lift coefficient of 0.51 is approximately 0.0317 which is 4.62% higher than wind tunnel model and maximum L/D is about 15.9 which is 7.5% lower than wind tunnel. For Pressure model with flow separation, drag coefficient for 0- and 1-degree angle of attack is lower, and it increased significantly after 2.5 degree of angle of attack compared to wind tunnel results. Drag coefficient at ideal lift for Pressure model is about 0.0302 and maximum L/D is

17.1 which is 0.33% and 0.4% respectively, lower than wind tunnel results. The drag count reduction for FlightStream FLAP1 model compared to baseline FLAP0 model is 2 for vorticity model and 17 for Pressure model with flow separation respectively.

4.1.3 FLAP2 Configuration Results:

In this configuration, deflections vary from maximum at the inboard and outboard flaps to minimum deflection at the mid-span flap. Total deflections from inboard to outboard flaps respectively are, 15°, 13°, 12°, 15°, 25° .
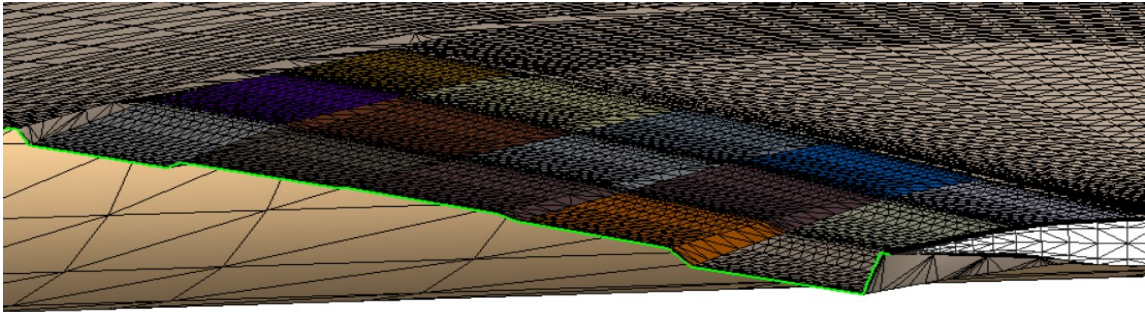

Figure 21: VCCTEF FLAP2 deflections
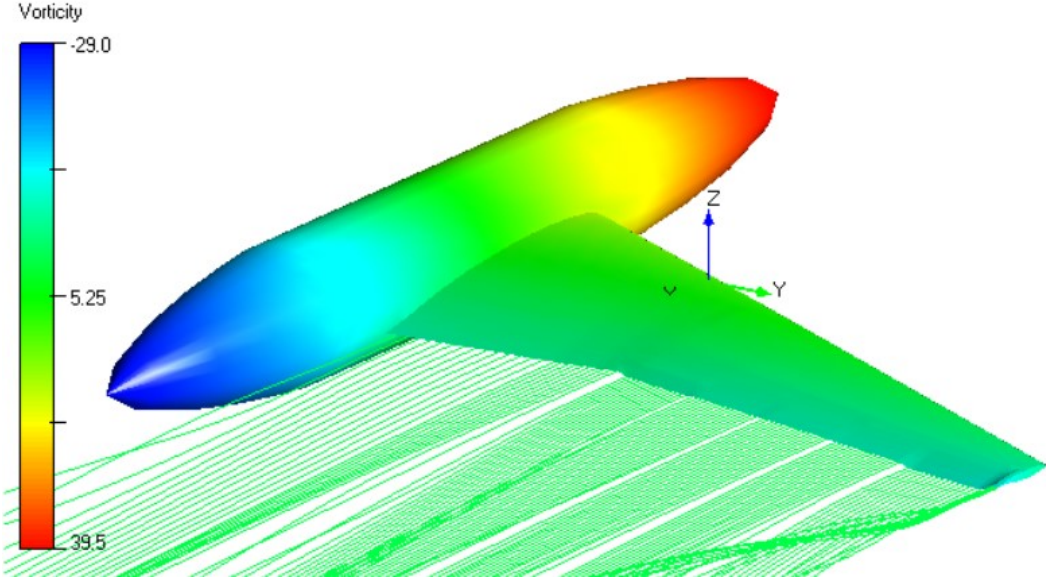
Figure 22: Vorticity distribution on FLAP2 configuration
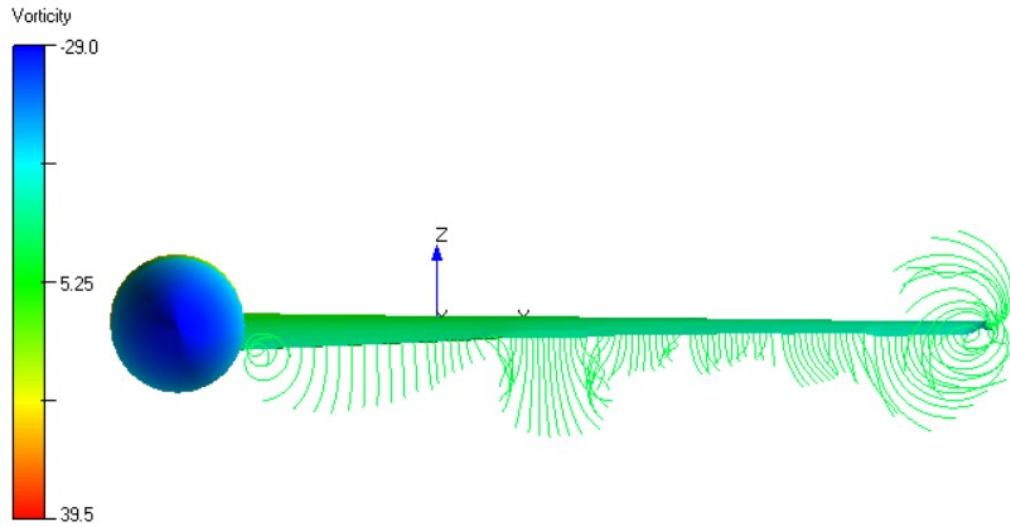
**Figure 23: Vortex shedding for FLAP2 configuration**
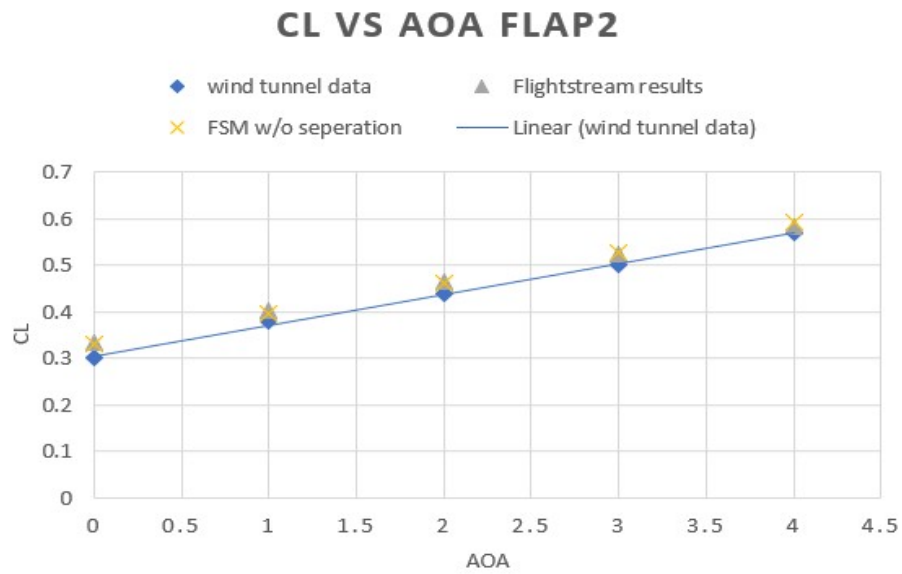
**Figure 26: Lift curve comparison for FLAP2**
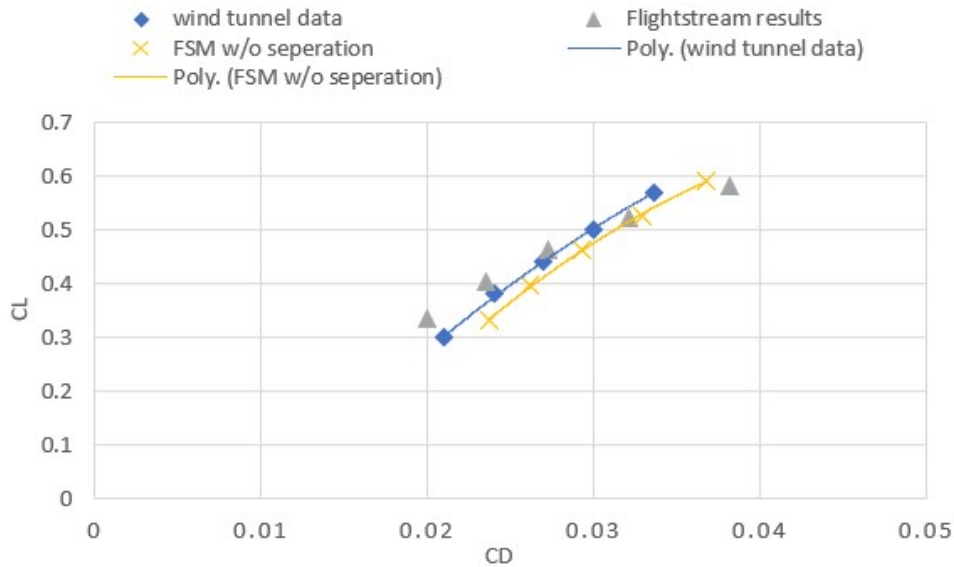
Figure 27: Drag Polar comparison for FLAP2

This configuration was run in FlightStream® for the two different loads and moments model, first with vorticity model and second with pressure model enabling turbulent transition as well as flow separation. FlightStream® overpredicted lift in both the cases compared to wind tunnel data. The vorticity model without turbulent transition and flow separation overpredicted drag for all values of angle of attack. However, with pressure model, turbulent transition and flow separation, drag generation on the model was lower than wind tunnel model for 0,1- and 2-degree angle of attack, but drag increased significantly for 3- and 4-degree angle of attack. Pressure based model solution is mesh sensitive. These results with flow separation are more likely to get better with improved mesh on the model. However, for vorticity-based solutions, vorticity can be used directly to calculate lift force using Kutta-Joukowski theorem while pressure is calculated based on the gradient of vorticity. To get a well resolved gradient of

vorticity, the mesh must be better refined. The drag coefficient at the ideal C_l of 0.51 obtained from vorticity model is about 0.0315 which is 4.65% higher than wind tunnel model and drag coefficient from pressure and flow separation model is about 0.0305 which is only 1.32% higher than wind tunnel. L/D max given by vorticity model is 16.07 which is 5.47% lower than wind tunnel data while L/D max given by pressure model with flow separation is 16.9 which is 0.58% lower than that of wind tunnel. The drag count reduction for this FlightStream® model configuration compared to baseline FLAP0 model is 4 for the vorticity model and 14 for the pressure model with flow separation.

4.1.4   FLAP3 Configuration Results:

In the FLAP3 configuration described in Table 2 in Chapter 3, the tab deflections vary from a minimum at the most inboard and the most outboard flaps to a maximum deflection at the midspan flap. The total deflections varying from inboard to outboard flaps respectively are 10°, 16°, 23°, 16°, and 15°.
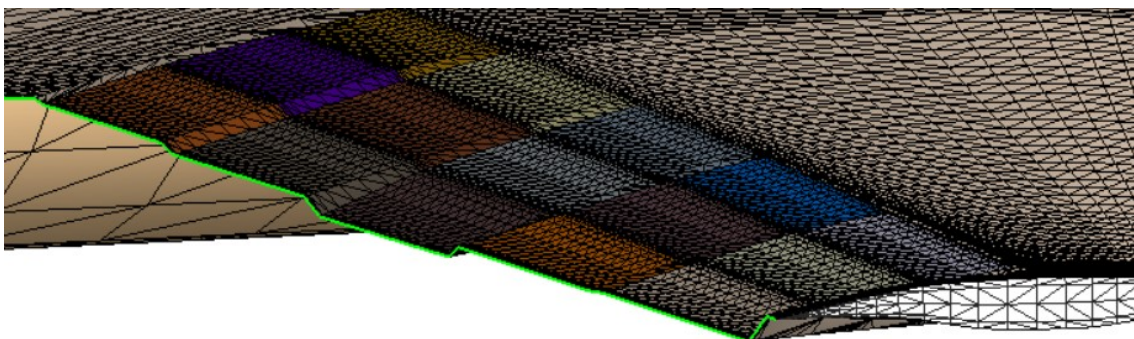

Figure 28: VCCTEF FLAP3 deflections
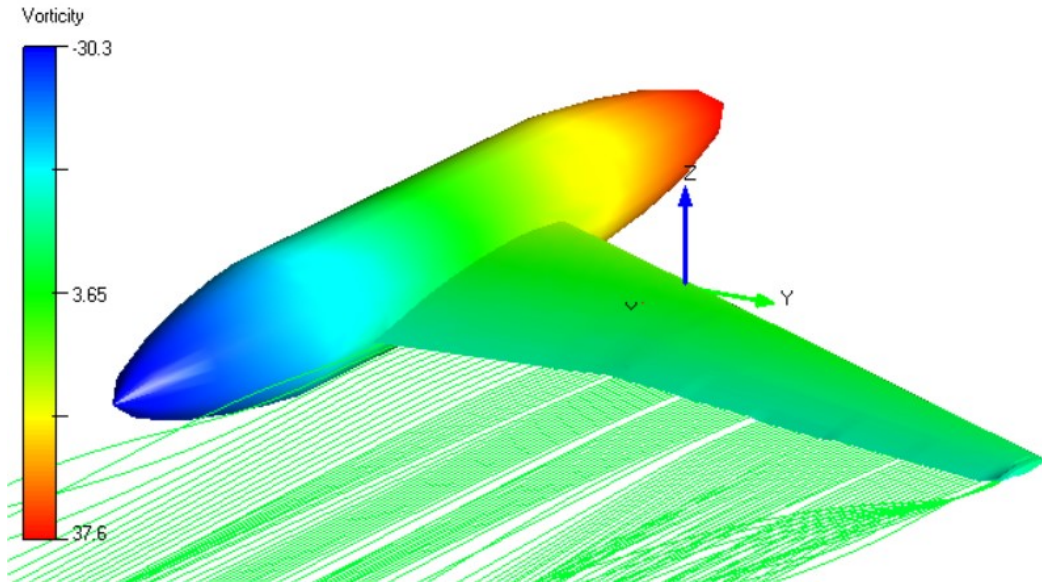
Figure 29: Vorticity distribution on FLAP3 configuration
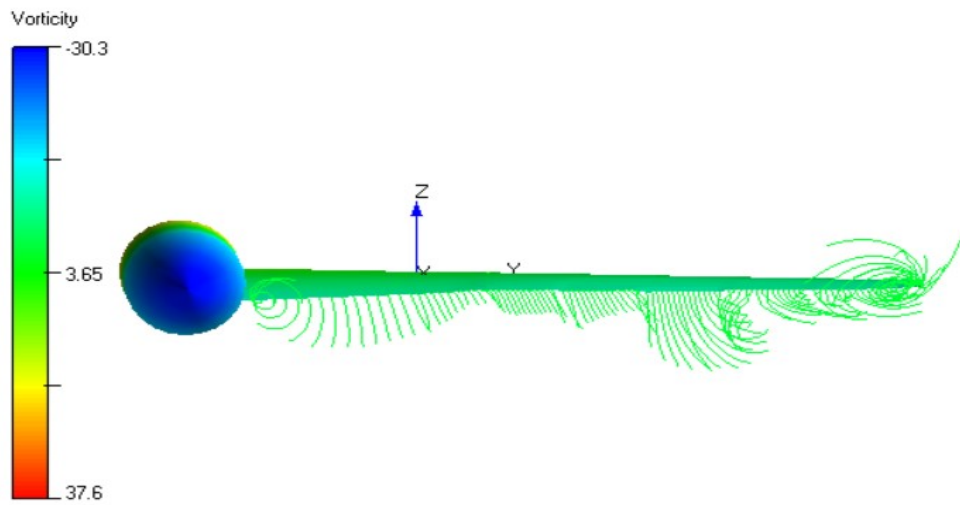

Figure 30: Vortex shedding for FLAP3
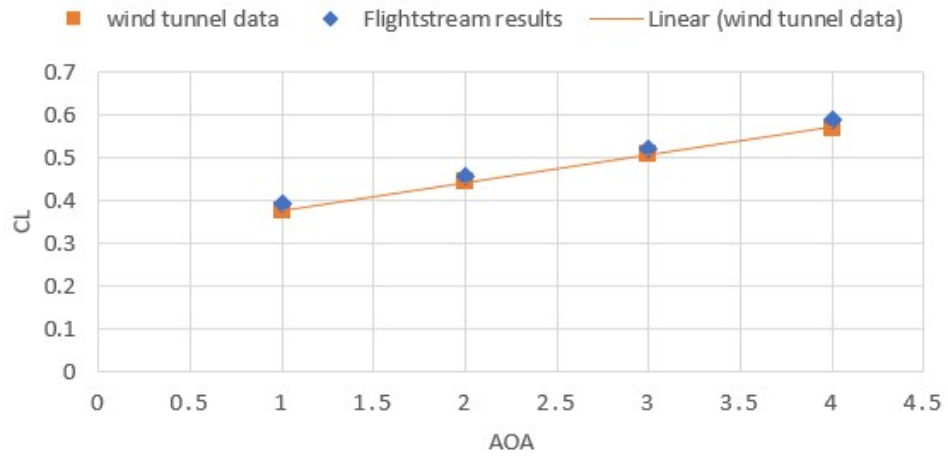
**Figure 31: Lift curve comparison for FLAP3 configuration**
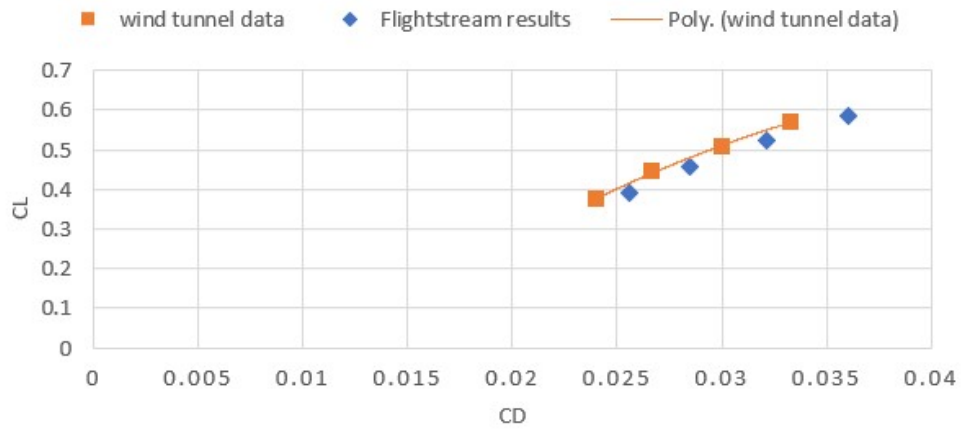
Figure 32: Drag Polar comparison for FLAP3 configuration

For this configuration, FlightStream® overpredicted the lift coefficients and hence the induced drag coefficients as compared to wind tunnel data. The drag coefficient at the lift coefficient value of 0.51 predicted by FlightStream® is about 0.0311 which is 3.6% higher than the wind tunnel data. Also, L/D max for the FlightStream model is 16.36 which is 4.67% lower than wind tunnel model. The FlightStream® data is still in agreement with wind tunnel data. Drag generation on FlightStream model at 4° angle of attack is much more than drag at 1°, 2° and 3° angle of attack. The results for 1°, 2° and 3° match much better with wind tunnel data. The total drag reduction count for FLAP3 configuration FlightStream® model compared to baseline FLAP0 FlightStream® model is 8. The solution was properly converged so the reasonable disagreements with the wind tunnel data are expected to be mostly due to geometry and mesh related issues. This geometry with every tab deflected at a different angle is especially susceptible to the triangulated meshes connecting the tabs.

4.1.5 FLAP4 Configuration Results:

The FLAP4 deflection case follows a pattern of monotonically varying deflections from maximum deflection at the inboard flap to zero deflection at the outboard flap. The total deflection from the inboard to outboard flaps respectively is 16 ^{o}, 12 ^{o}, 11 ^{o}, 9 ^{o}, and 0 ^{o}. Figure 33 shows FlightStream® deflected FLAP4 model and Figure 34 shows the vorticity distribution and the vortex shedding of the model. Figure 36 and 37 show validation results for the FLAP4 case.
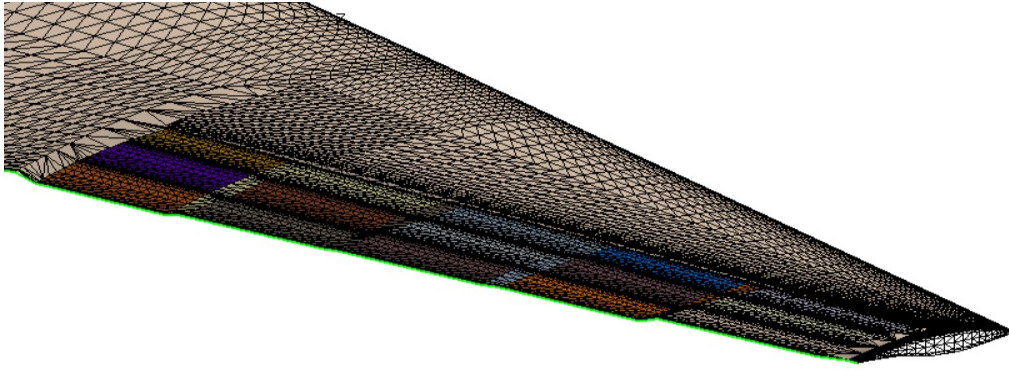
Figure 33: VCCTEF FLAP4 deflections
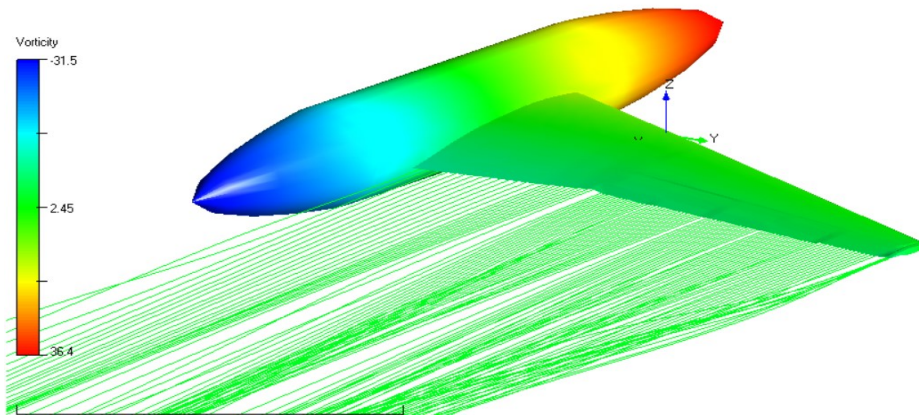
Figure 34: Vorticity distribution FLAP4 model
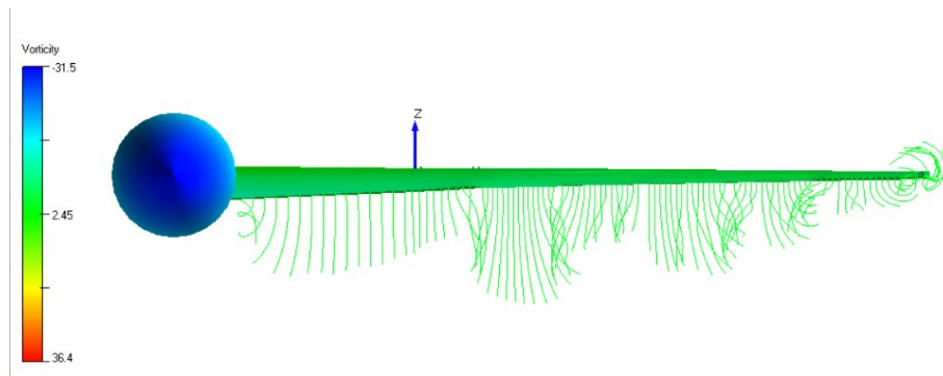
Figure 35: Vortex shedding FLAP4 model
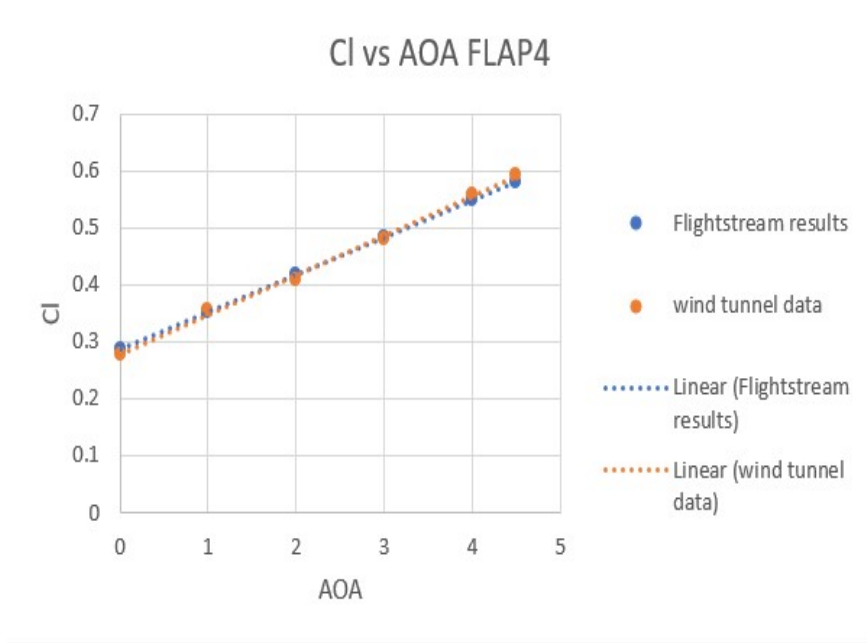
Figure 36: Lift curve comparison for FLAP4
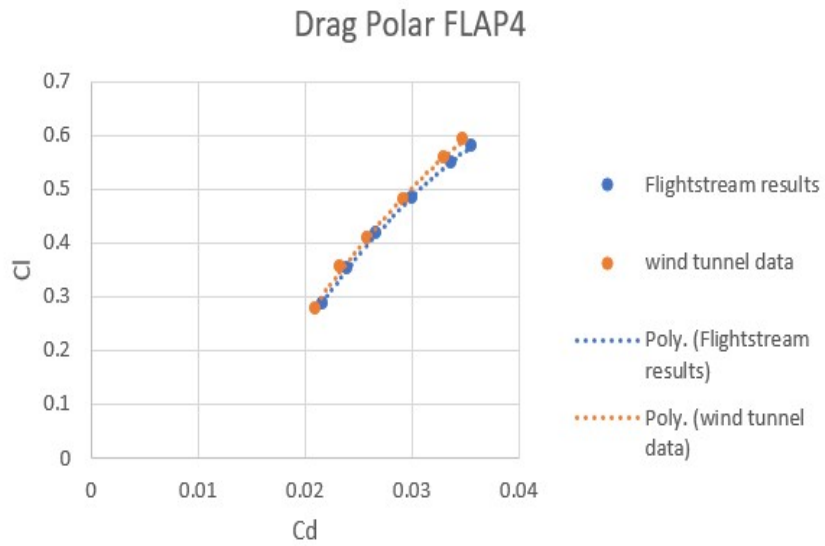
Figure 37: Drag Polar comparison for FLAP4

According to graphs shown in Figure 36 and 37, the results obtained with FlightStream®
agree well with the wind tunnel data. C_d value at lift co-efficient of 0.51 for FlightStream®
results is at 0.0311 while for wind tunnel model it's at 0.0308 yielding an error of only 0.96%.
The total drag reduction count for FLAP4 configuration FlightStream® model compared to
baseline FLAP0 FlightStream® model is 8.

4.1.6 FLAP5 Configuration Results:

For the FLAP5 configuration, deflections vary monotonically from zero at the inboard flaps
to maximum at the outboard flaps. The total deflection angles of the flaps from inboard to
outboard respectively are, 0 º, 8 º, 13 º, 14 º, and 20 º. Figure 38 shows deflections of
FlightStream model.
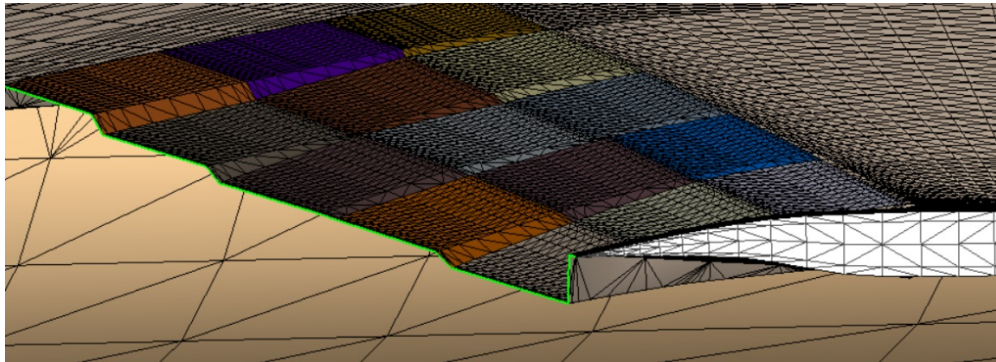
Figure 38: VCCTEF FLAP5 deflections
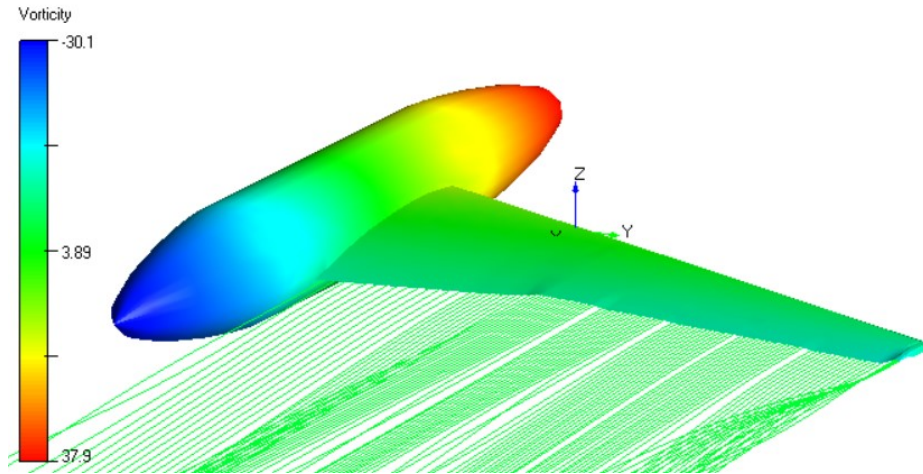
Figure 39: Vorticity distribution on FLAP5 configuration
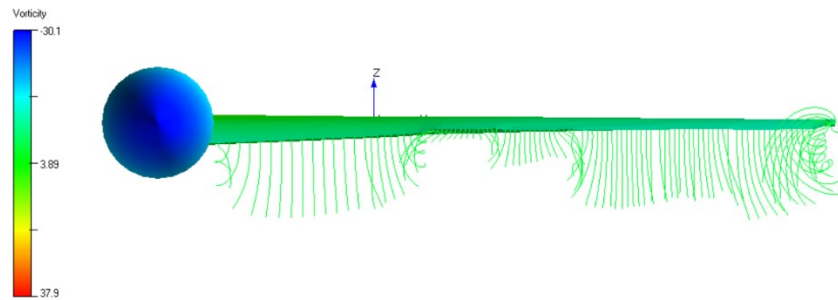
Figure 40: Vortex shedding for FLAP5 configuration
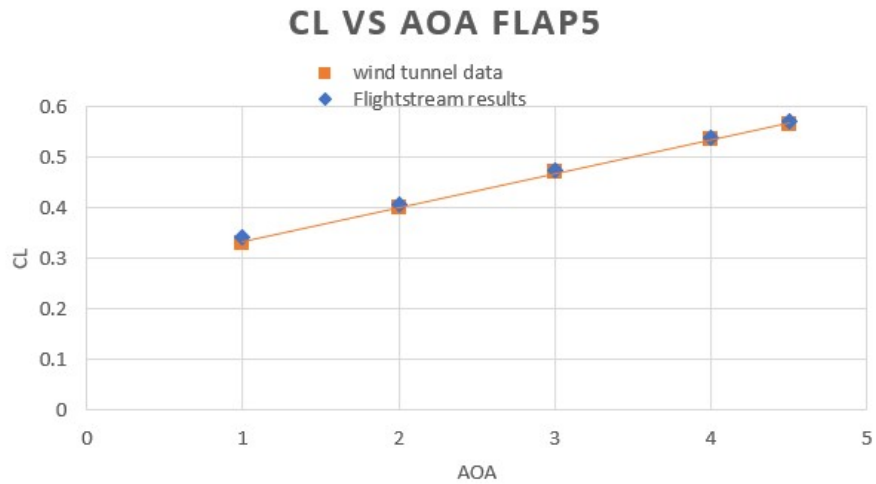
Figure 41: Lift curve comparison for FLAP5
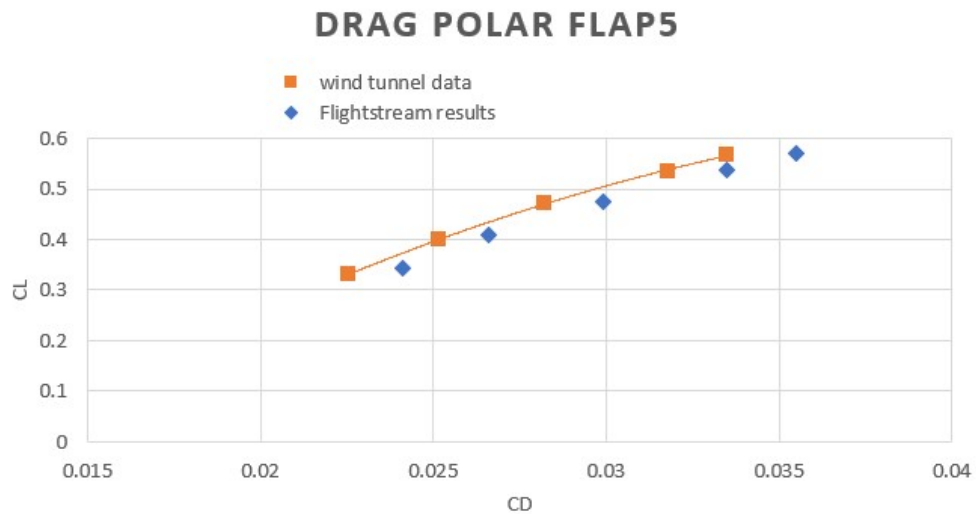
Figure 42: Drag Polar comparison for FLAP5

For this configuration, FlightStream® slightly over predicted drag as compared to the wind tunnel results. However, the lift curve solution obtained in FlightStream® agrees well with

the wind tunnel data. The drag coefficient at design lift coefficient value of 0.51 is 0.0317 for the FlightStream® model, 3.93% higher than wind tunnel result. The L/D max for the FlightStream® model is about 16.1, or 4.73% lower than wind tunnel results. The drag count reduction compared to baseline FLAP0 FlightStream® model achieved by FLAP5 FlightStream® model is 2, small in comparison to some of the other configurations.

4.1.7 FLAP6 Configuration Results:

The FLAP6 deflection pattern is similar to the FLAP4 case, but with smaller deflection angles. Total deflections of flap sets from inboard to outboard flaps respectively are 3 $^{\circ}$, 2 $^{\circ}$,2 $^{\circ}$, 0.5 $^{\circ}$ and 0 $^{\circ}$. Figure 20 shows the shape of the wing with these flap deflections. Figure 43 shows FlightStream FLAP6 deflection model.
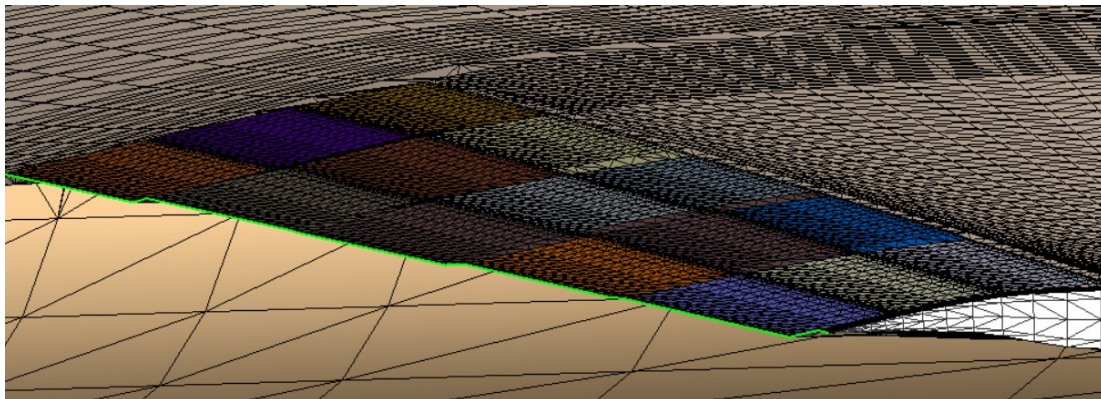
Figure 43: VCCTEF FLAP6 deflections
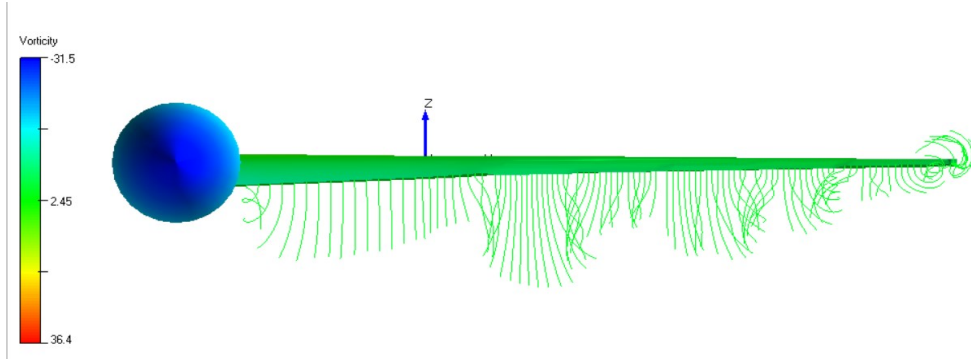
Figure 44: Vortex shedding FLAP6
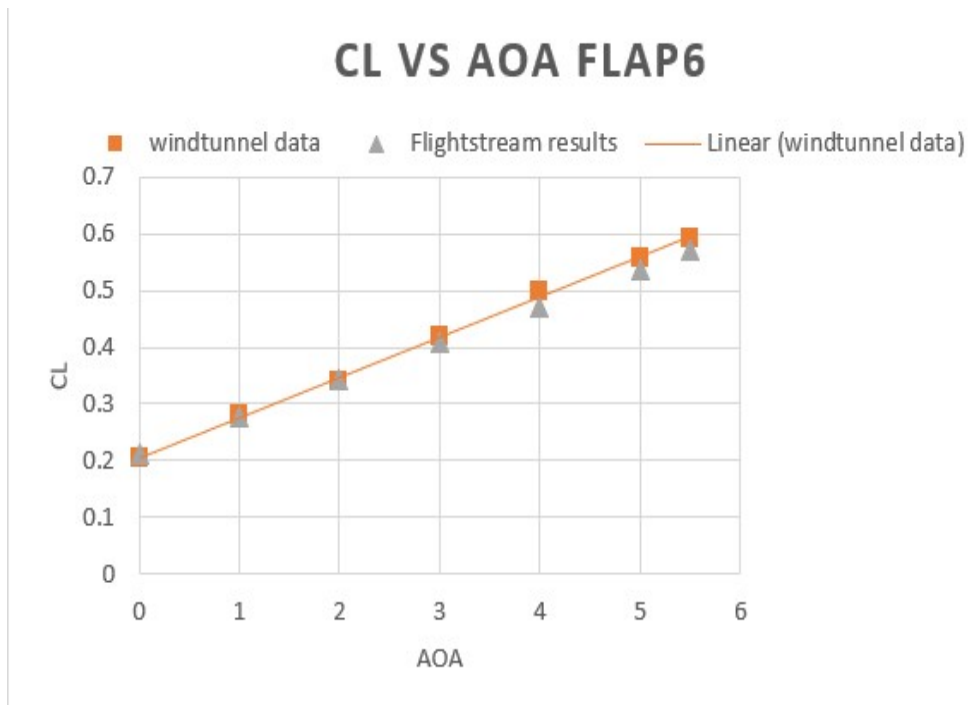
Figure 45: Lift curve comparison for FLAP6

DRAG POLAR FLAP6
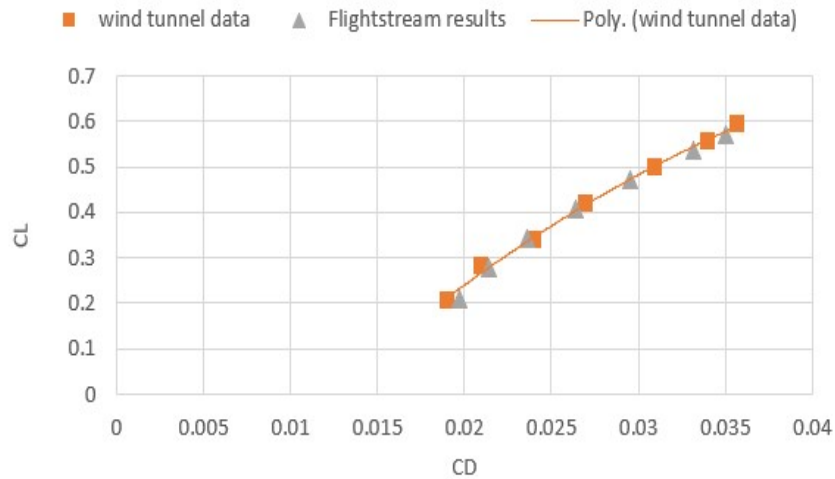
Figure 46: Drag Polar comparison for FLAP6

Figures 45 and 46 shows comparison of FlightStream® results with Wind Tunnel data. FlightStream® results agree well with wind tunnel data. The drag coefficient at lift coefficient of 0.51 for FlightStream® analysis is turned out to be approximately about 0.0314, which is 0.32% higher than the C_d obtained in wind tunnel data. Similarly, maximum L/D obtained by FlightStream® analysis is 16.3 which is 1.8% lower than wind tunnel data value. The drag count reduction between FLAP0 and FLAP6 configuration at C_l of 0.51 is observed to be 5 which proves the trends are correct, and the results agree with the wind tunnel data as well as can reasonably be expected for a conceptual design level analysis.

4.1.8 FLAP7 Configuration Results:

In this case, deflections vary monotonically from maximum positive deflection at inboard flap to negative deflections at the outboard flap. The total deflection angles from inboard to outboard respectively are 10 $^\circ$, 7 $^\circ$, 3 $^\circ$, 0 $^\circ$, and -2 $^\circ$. Figure 47 shows the FLAP7 deflection configuration, Figure 48 shows the vorticity distribution and vortex shedding. A comparison between the analysis and wind tunnel data is presented in Figure 50 and 51.
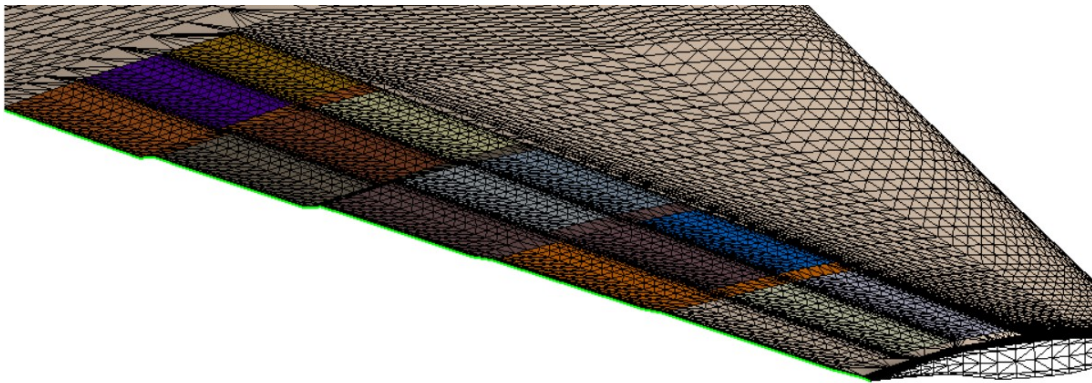
Figure 47: VCCTEF FLAP7 deflections
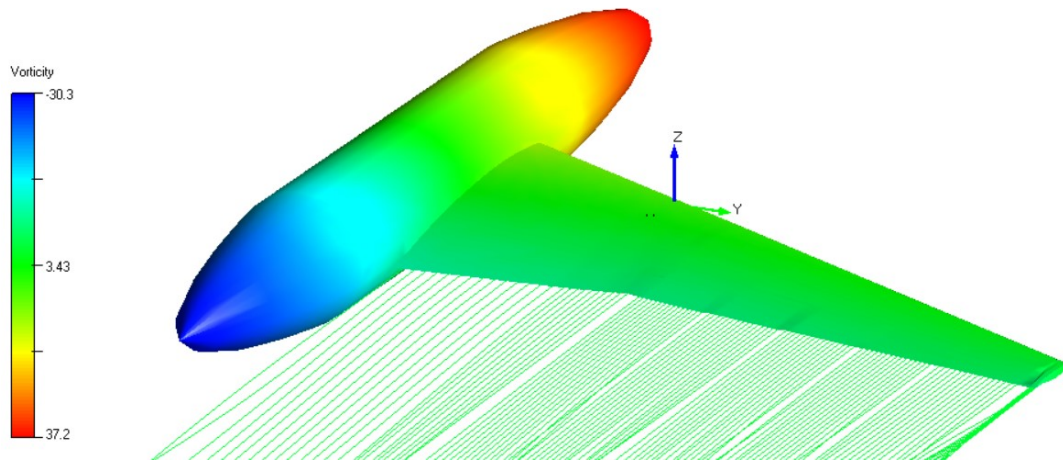
Figure 48: Vorticity distribution on FLAP7 configuration
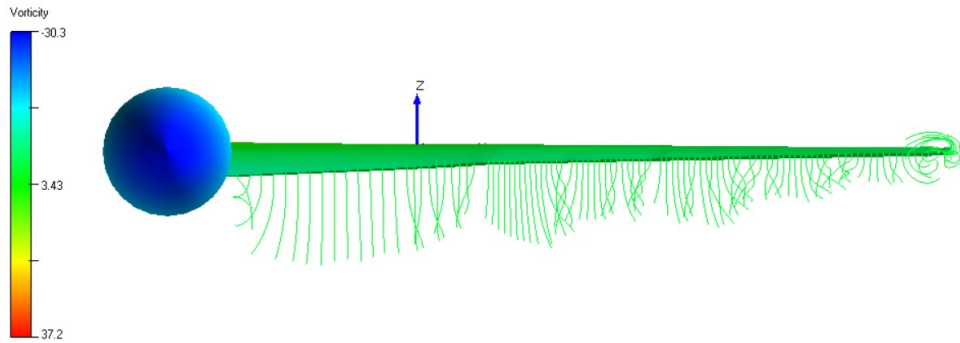
Figure 49: Vortex shedding FLAP7 configuration
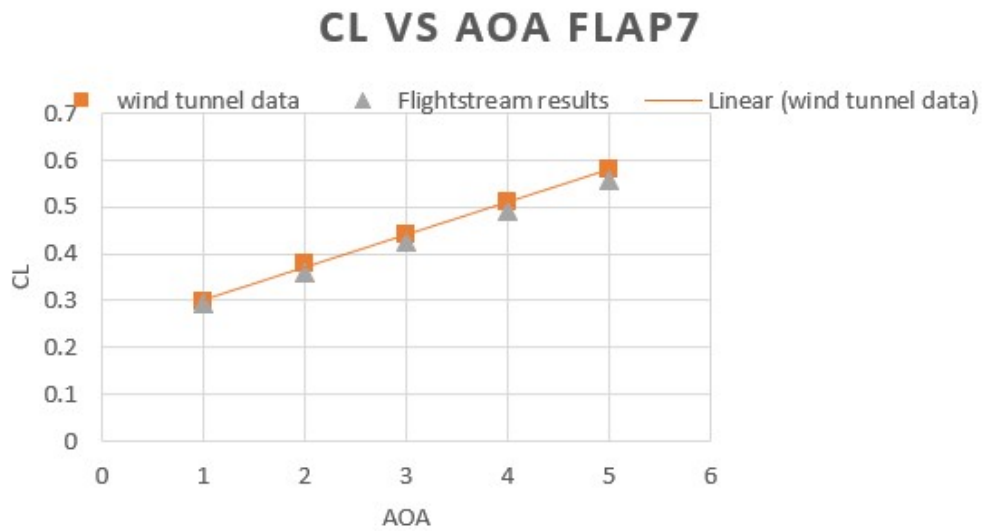
Figure 50: Lift Curve comparison for FLAP7 configuration
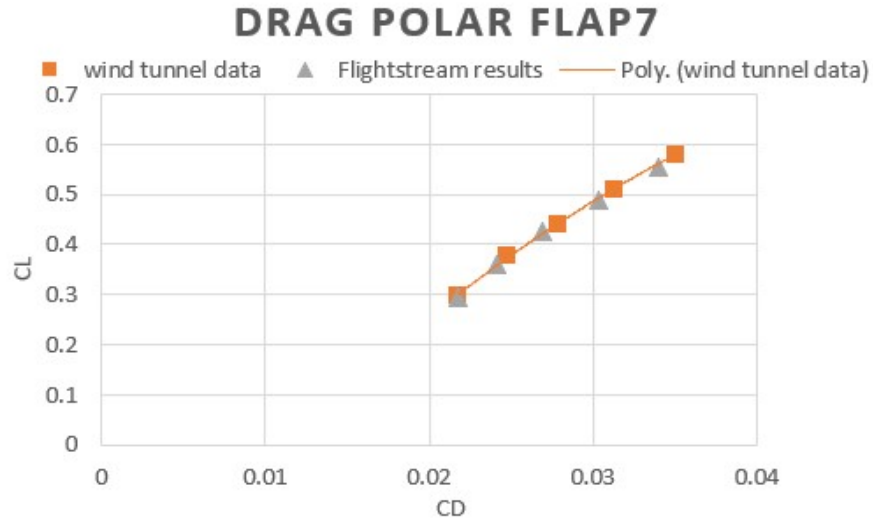
Figure 51: Drag Polar comparison for FLAP7 configuration

These results for lift and drag showcase again excellent overall agreement between FlightStream® and the wind tunnel data. The lift coefficient dropped by a 4.3% at 5° angle of attack due possibly to viscous effects do not capture in the modeling. As of this writing, FlightStream® does not have a boundary layer displacement model and in this configuration, it is possible that increasing boundary layer thicknesses on the upper surface as compared to the lower surface has the effect of decreasing the effective angle of attack. The drag coefficient at C_l of 0.51 for FlightStream® analysis is approximately 0.0314, which is 0.319% higher than wind tunnel value. L/D max as obtained from FlightStream® analysis is 16.321, around 1.85% lower than wind tunnel value. Notice that the drag reduction at C_l value of 0.51 for FlightStream® models FLAP0 and FLAP7 case is 5, illustrating a drag reduction improvement for the morphed wing even if crudely morphed.

4.1.9 FLAP8 Configuration Results:

In the FLAP8 case, the deflections are rigid body deflections with two outer camber segments at zero relative deflection. The total deflections from inboard to outboard flap segments are $4\,^{o}$, $4\,^{o}$, $5\,^{o}$, $5\,^{o}$, and $4\,^{o}$. The resulting geometry is depicted in Figure 52.
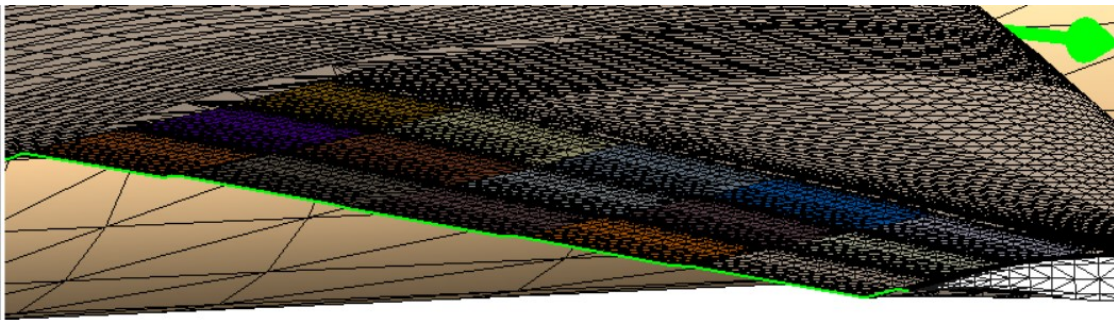

Figure 52: VCCTEF FLAP8 configuration
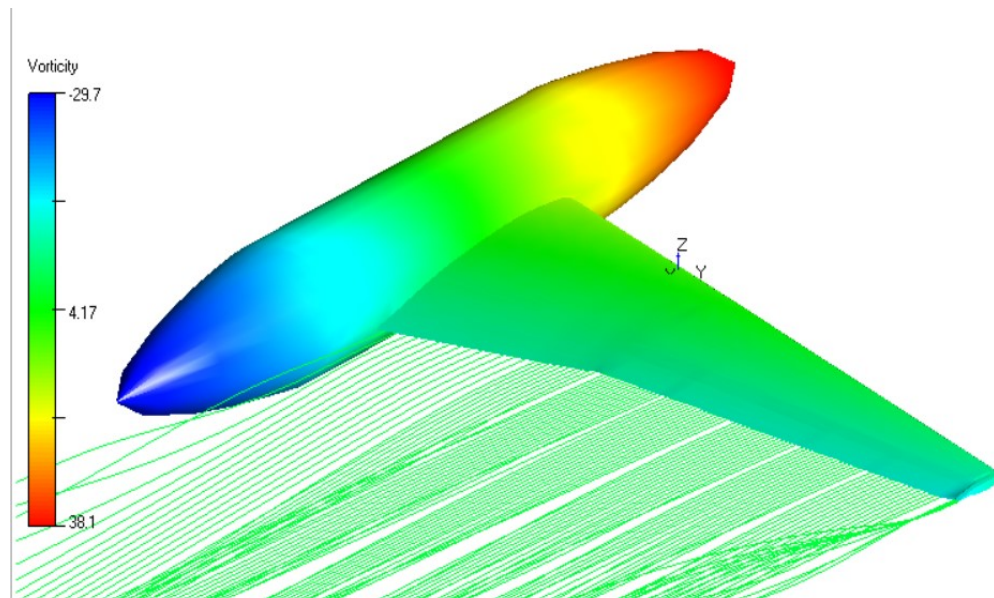
**Figure 53: Vorticity distribution for FLAP8 configuration**
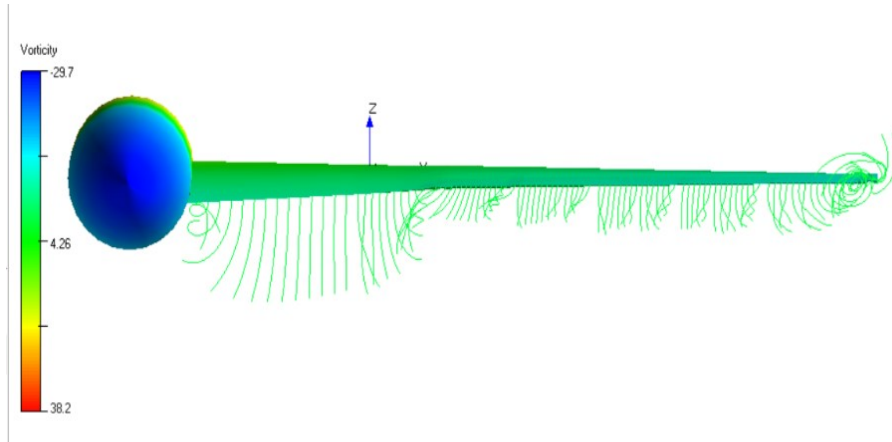
Figure 54: Vortex shedding for FLAP8
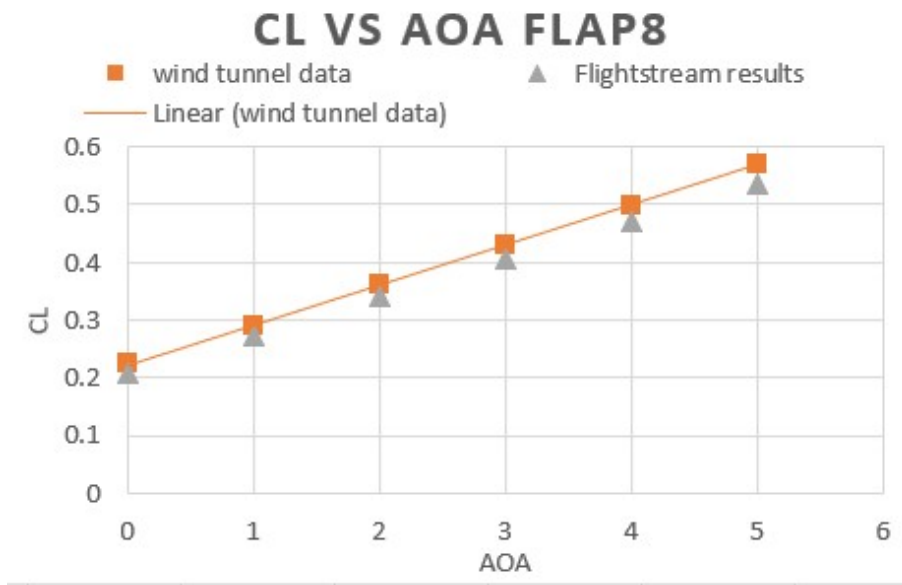

Figure 55: Lift curve comparison for FLAP8 configuration
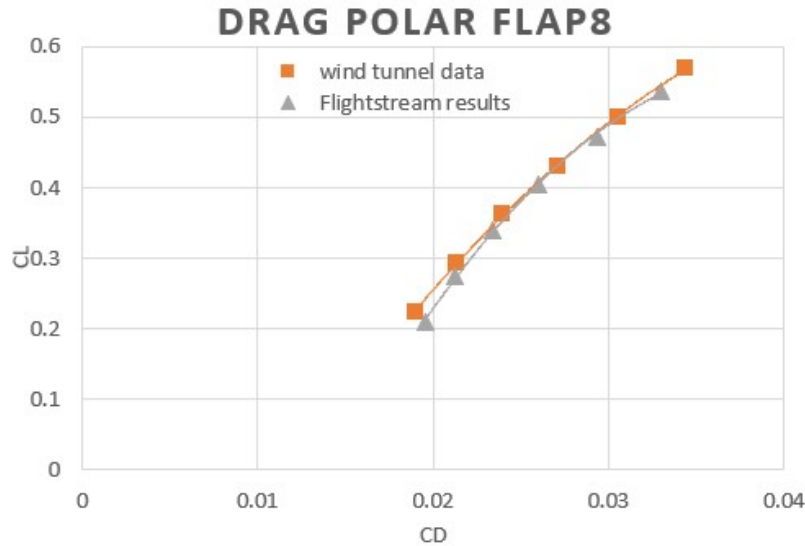
Figure 56: Drag Polar comparison for FLAP8 configuration

The comparative analysis shown in Figures 55 and 56 illustrate a very effective aerodynamic prediction capability for FlightStream®. The lift from the FlightStream® model is slightly lower for all values of angle of attack as compared to wind tunnel data. The drag coefficient calculated by FlightStream® at C_l of 0.51 is about 0.0314 which is 0.96% higher than wind tunnel result for this configuration. L/D max for FlightStream® model is 2.814% lower than wind tunnel model. The drag count reduction between FLAP0 and FLAP8 configuration at C_l value of 0.51 is observed to be 5. Again, the trends are correct, and the results agree with the wind tunnel data as well as can reasonably be expected for a conceptual design level analysis.

4.1.10 FLAP9 Configuration Results:

In the FLAP9 case, only the trailing edge segments are deflected. The deflection angles of the segments are $6°$, $6°$, $8°$, $6°$, and $6°$. Figure 57 shows resulting geometry.
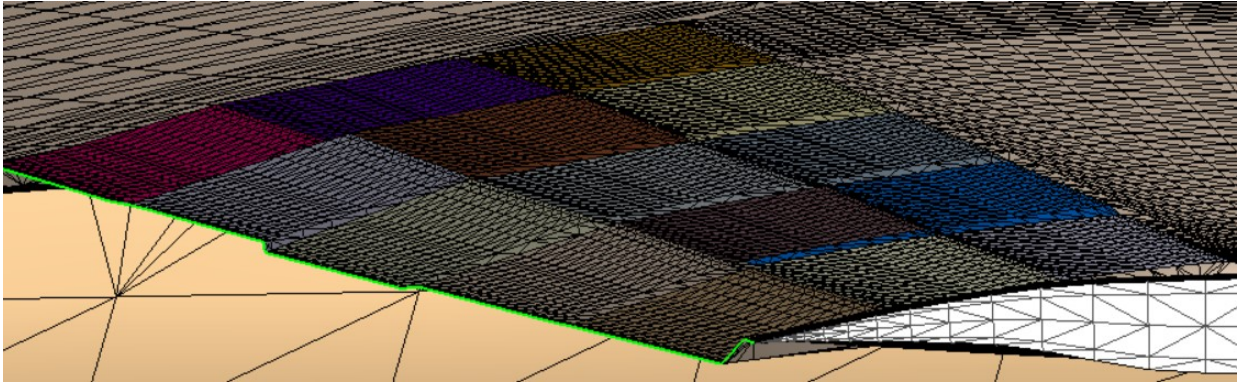
Figure 57: VCCTEF FLAP9 deflections
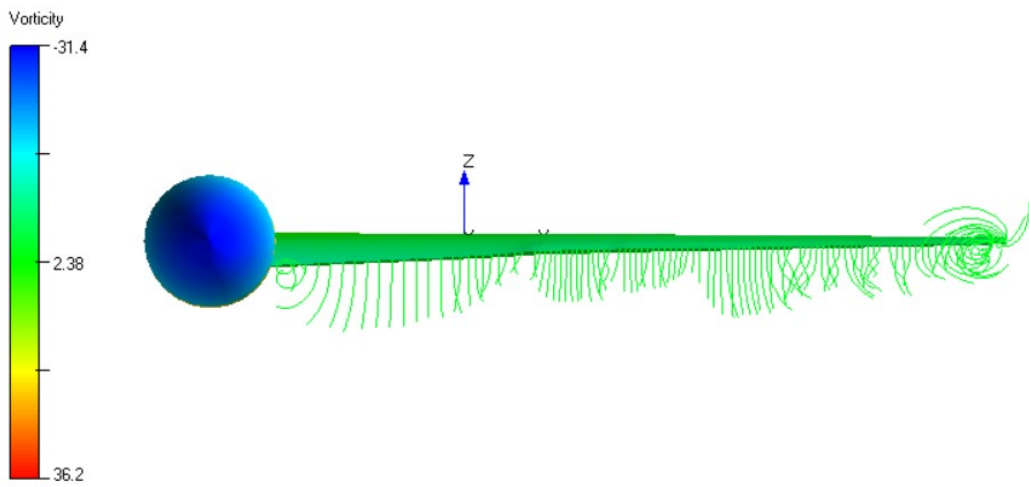
Figure 58: Vortex shedding for FLAP9 configuration
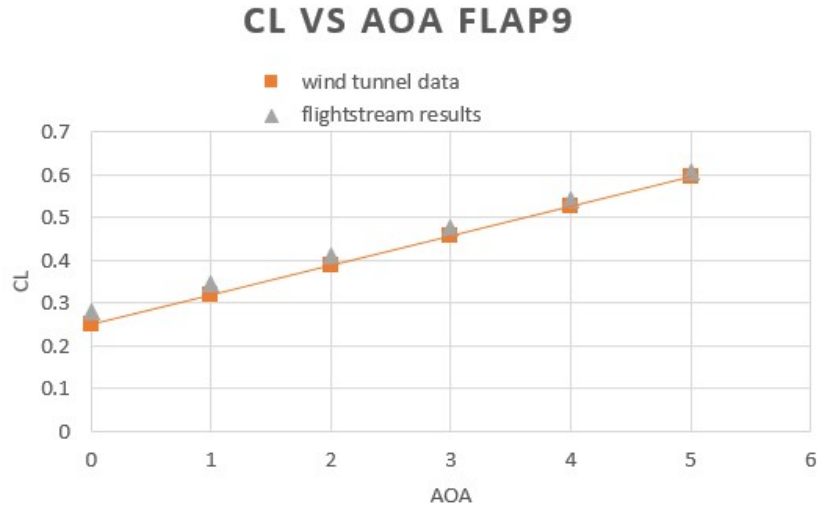
Figure 59: Lift curve comparison for FLAP9 configuration
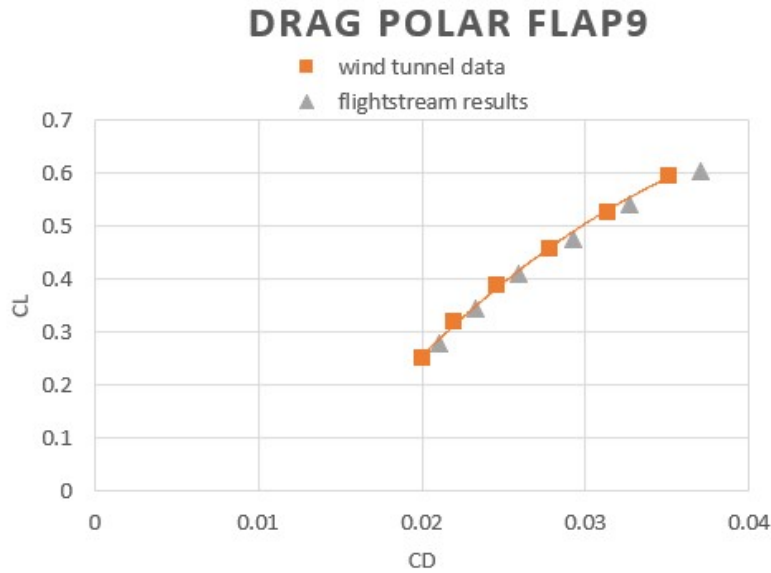
Figure 60: Drag Polar comparison for FLAP9 configuration

The comparative analysis shown in Figures 59 and 60 illustrate a very effective aerodynamic prediction capability for FlightStream®. The lift from the FlightStream® model is

slightly higher than wind tunnel data. The drag coefficient calculated by FlightStream® at C_1 of 0.51 is about 0.0310 which is 1.61% higher than wind tunnel result for this configuration. L/D max for FlightStream® model is 2.61% lower than wind tunnel model. The drag count reduction between FLAP0 and FLAP9 configuration at C_1 0.51 is observed to be 9. Again, the trends are correct, and the results agree with the wind tunnel data as well as can reasonably be expected for a conceptual design level analysis.

4.1.11 FLAP10 Configuration Results:

In the FLAP10 case , all the flaps are at intermediate deflection angle. Total deflections for flap starting from inboard to outboard flap sets are 7°, 7°, 11°, 9°, and 10° respectively.
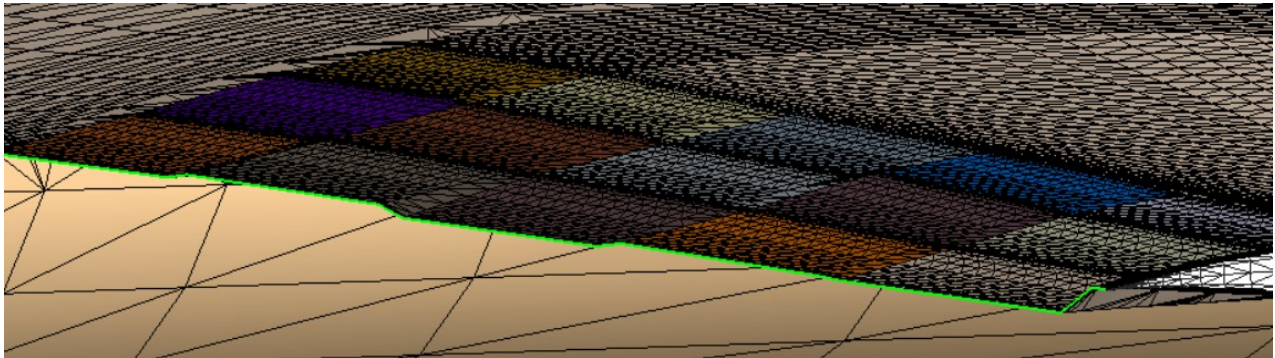
Figure 61: VCCTEF FLAP10 deflections
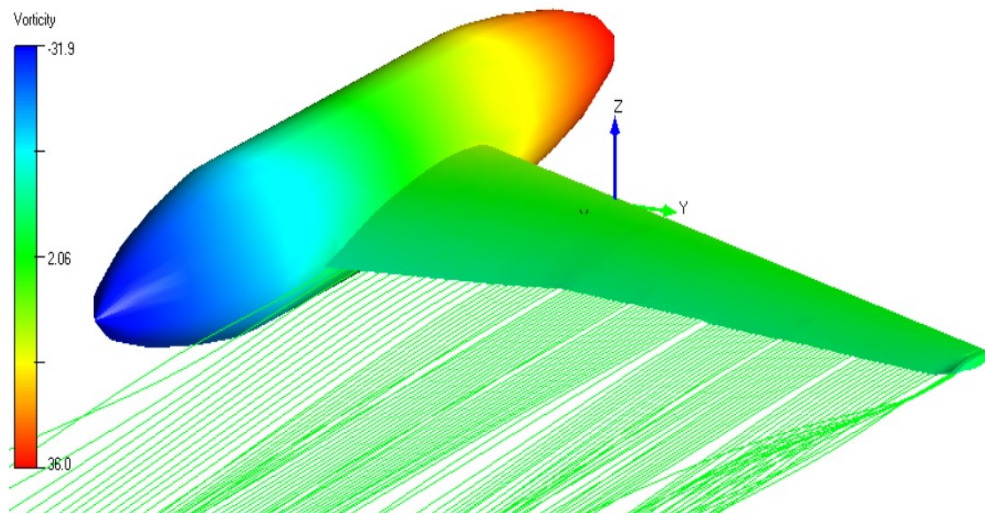
Figure 62: Vorticity distribution FLAP10
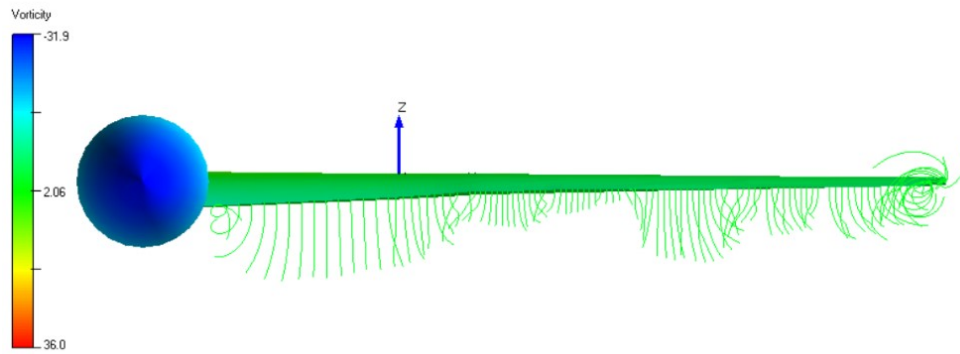
Figure 63: Vortex shedding FLAP10
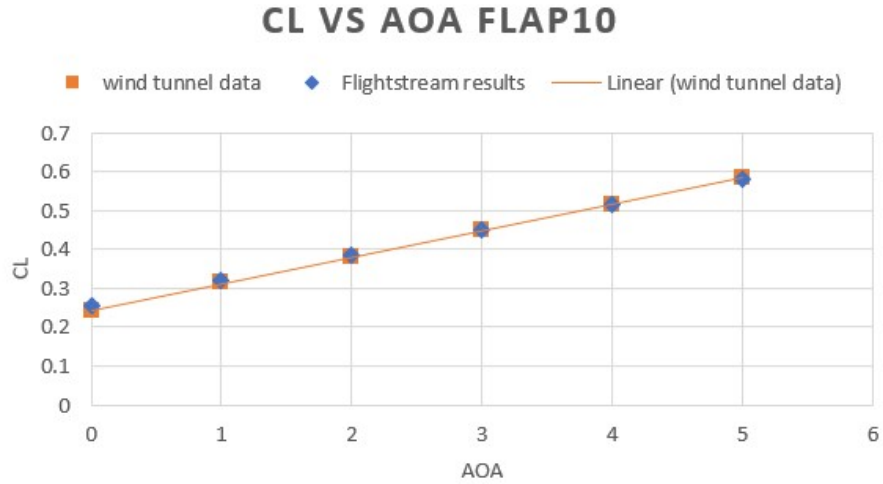
Figure 64: Lift curve comparison FLAP10
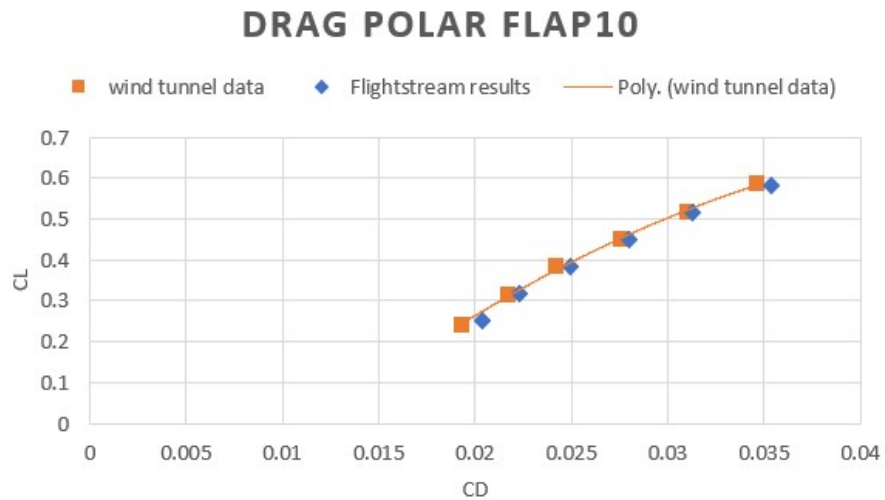
Figure 65: Drag Polar comparison FLAP10

The data shown in Figures 64 and 65 illustrate a compelling ability to use a lower order surface vorticity model such as FlightStream® to develop aerodynamic performance data for proposed configurations. The FlightStream® Solution was fully converged on a relatively course

surface mesh. The drag coefficient from FlightStream® at C_l of 0.51 for this configuration is about 0.0311, which is 1.3% higher than the wind tunnel data. L/D max from FlightStream® is 16.45, or 2.9% lower than wind tunnel value. Also, the drag count reduction achieved by this configuration compared to baseline FLAP0 FlightStream® model at the C_l of 0.51 is 8, again illustrating both the utility of the morphing wing concept and the ability of FlightStream® to capture the trends in wing morphing to drive a design to an ideal configuration very quickly at the conceptual design phase.

4.1.12 FLAP11 Configuration Results:

The FLAP11 configuration is the last VCCTEF model tested for the validation exercise. This is complete negative deflection configuration. The total deflections of the flap from inboard to outboard respectively are -4 °, -6 °, -5 °, -7 °, and -8 °. Due to the negative deflections, lift is lower resulting in more drag generation on the model compared to the baseline FLAP0 configuration.
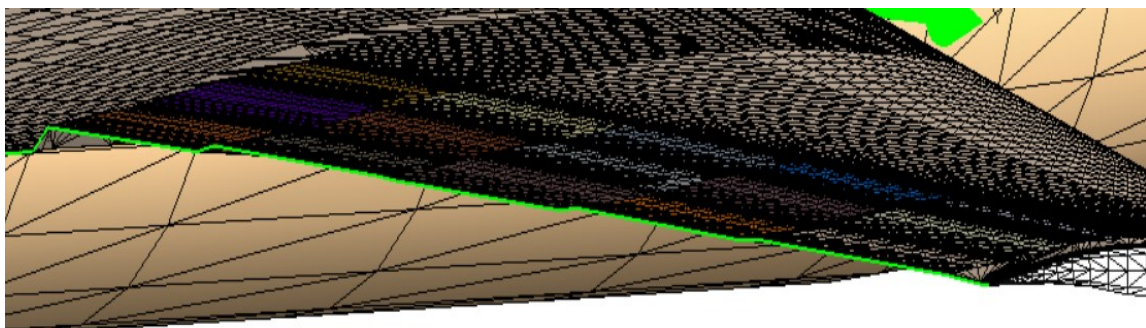
Figure 66: VCCTEF FLAP11 deflections
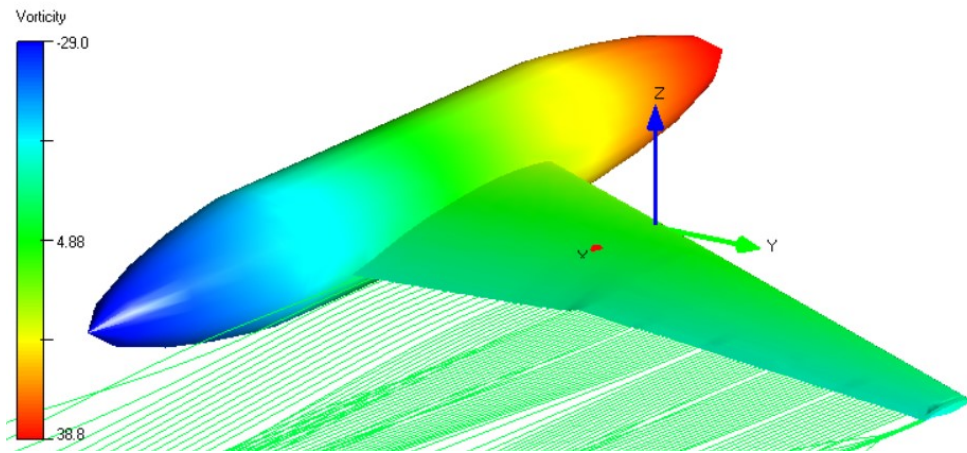
Figure 67: Vorticity Distribution FLAP11
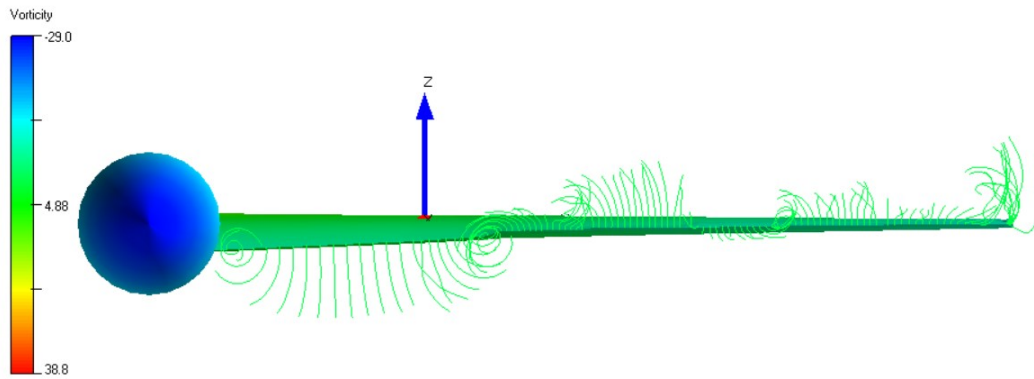
Figure 68: Vortex shedding FLAP11

CL VS AOA FLAP11
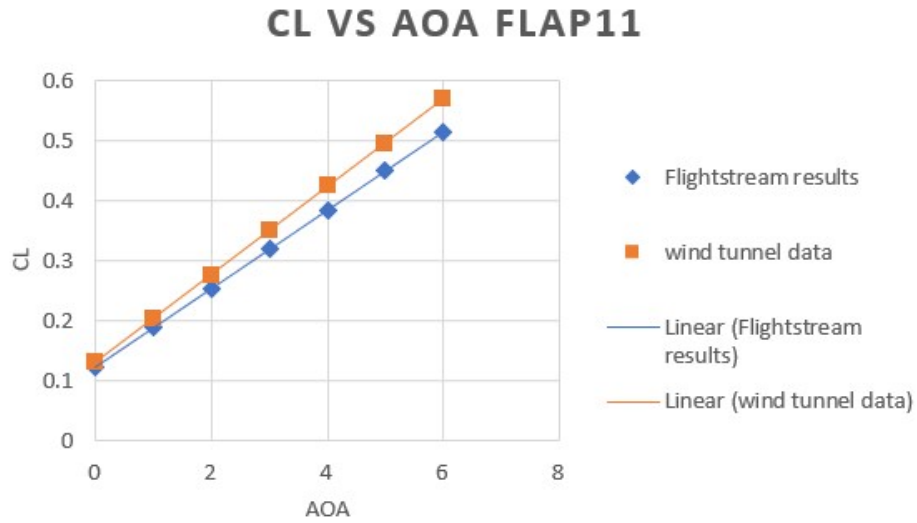
Figure 69: Lift curve comparison FLAP11
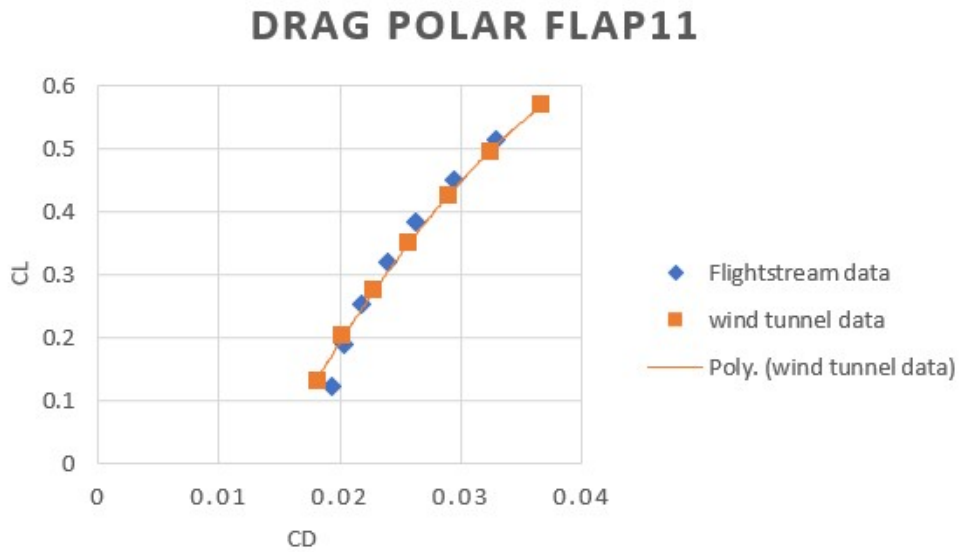
DRAG POLAR FLAP11

Figure 70: Drag polar comparison FLAP11

With negative flap deflections, the FlightStream® lift slope is substantially perceptibly lower than indicated by the wind tunnel. This is likely due to the expected very thick boundary

layer on the upper surface as compared to the lower surface, which will very likely be exacerbated increasingly at ever more elevated angles of attack. Nevertheless, the FlightStream® results presented in Figure 58 a and b agree in aggregate with the wind tunnel results. The drag coefficient at C_l of 0.51, for FlightStream® model is about 0.0329 which is 0.604% lower and maximum L/D is 15.65 which is 0.571% lower than wind tunnel results. Due to negative deflections, drag count increased for this FlightStream® configuration compared to baseline FLAP0 FlightStream® model by 10. This configuration is not aerodynamically efficient and does not support the concept of drag reduction using the VCCTEF Flexible Wing concept.

4.2   Summary of validation results and possible explanation for observed errors:

Most of the results listed in section 4.1 for all 12 FlightStream models are overall in excellent agreement with the wind tunnel results. In most of the FlightStream cases, at high angle of attack, FlightStream underpredicts lift slightly which might be due to increase in boundary layer. All the FlightStream solutions, vorticity, lift, induced drag and moments were converged properly, to residual vorticity of 200%, and the solution error is within 5% and is much less in most configurations. Drag is overpredicted somewhat on the models with high flap deflections. FLAP1, FLAP2, FLAP3 and FLAP5 are the high deflection configurations with at least one flap set undergoing total deflection of 20° or more. In the remaining configurations, the total flap deflections are under 20°.

The additional drag generation for the FlightStream models (Especially high deflection cases) might be due to the problem at flap attachment to the fixed wing and between each element. The mesh repair and flap deflections were completed manually and might contain a slightly uneven surface at the attachment section. The high lift configurations would be sensitive

to such geometric imperfections. Only the planform of wind tunnel model was used to design model as given in the reference 1, but the exact airfoil co-ordinates and twist on the fixed wing were not precisely known, thereby leaving some additional margin for geometric error. The mesh generated after connecting all the flaps to each other and to the fixed wing to form a continuous trailing edge and main wing leading edge mesh might need to be refined in order to improve results. In wind tunnel analysis, half fuselage with 6-inch radius is used while FlightStream model has full fuselage with maximum 12-inch diameter. Even though it does not contribute to lift and induced drag, but it affects the C_{d0} value.

Table 3 shows the summary of the validation results calculated using Vorticity Loads and moments model. The main purpose of VCCTEF concept is to reduce drag which is successfully achieved by VCCTEF flexible wing FlightStream® models. Table 3 shows comparison for C_d at C_l value of 0.51 and maximum L/D for wind tunnel data and FlightStream® results. This table also presents drag count reduction for each VCCTEF FlightStream® model compared to the FlightStream® baseline FLAP0 model. Wing morphing is an excellent and viable solution for midflight fuel optimization, lift, load affiliation, pitch, roll and yaw control. The shape of conventional aircraft is only optimized for one flight condition while morphing wing aircraft allows for active shape change under different flight conditions, which can provide additional aerodynamic performance benefits [22]. Due to morphing wing's ability to reduce overall drag on the aircraft, shape of the wing could be changed during cruise prioritizing fuel efficiency. VCCTEF wing can be morphed into different configurations and is advantageous wing shape for every stage of flight and analysis results proved ability of FlightStream to capture this trend in a very computationally efficient manner.

Table 3: Summary of Validation Results

	C_d at 0.51 C_l WTD	Max L/D WTD	C_d at 0.51 C_l FSM	Max L/D FSM	%C_d difference	% Max L/D difference	Cd count reduction FSM
FLAP0	0.0317	16.41	0.0319	16.11	0.63	1.82	0
FLAP1	0.0303	17.2	0.0317	15.9	4.62	7.55	2
FLAP2	0.0301	17	0.0315	16.07	4.65	5.47	4
FLAP3	0.03	17.12	0.0311	16.36	3.6	4.67	8
FLAP4	0.0308	16.81	0.0311	16.328	0.964	2.86	8
FLAP5	0.0305	16.9	0.0317	16.1	3.93	4.73	2
FLAP6	0.0313	16.6	0.0314	16.3	0.319	1.8	5
FLAP7	0.0313	16.63	0.0314	16.321	0.319	1.858	5
FLAP8	0.0311	16.7	0.0314	16.23	0.964	2.814	5
FLAP9	0.0305	16.98	0.031	16.529	1.61	2.65	9
FLAP10	0.0307	16.94	0.0311	16.45	1.3	2.89	8
FLAP11	0.0331	15.74	0.0329	15.65	0.604	0.571	-10

(1 count = 0.0001)

Only two results are more than 5% off. this is possibly due to mesh issues occur in cases which are very difficult for potential solvers to deal with. Most results are 2-3% and trends are all captured correctly, yielding an excellent validation case for a conceptual design level solver. Also, L/D improvements listed in table 3 are applicable to low speed flow without considering full configuration with pitch trim and thrust effect. High speed flow as well as contribution of vertical and horizontal tail can influence performance of VCCTEF Flexible Wing [1].

Chapter 5

Conceptual Morphing Wing Demonstration : Geometry

5.1   Open VSP Model:

Full span GTM equipped with VCCTEF for wing shaping control is shown in figure 71. This is the refined morphing wing geometry given in reference 1. It has 3 chordwise flap sections and 14 spanwise flaps and 3 flaps on the fixed wing section. The detailed geometry or test conditions are not mentioned in the paper. Referring this design, conceptual model completed in FlightStream has 15 spanwise flaps but only 1 chordwise flap segment.
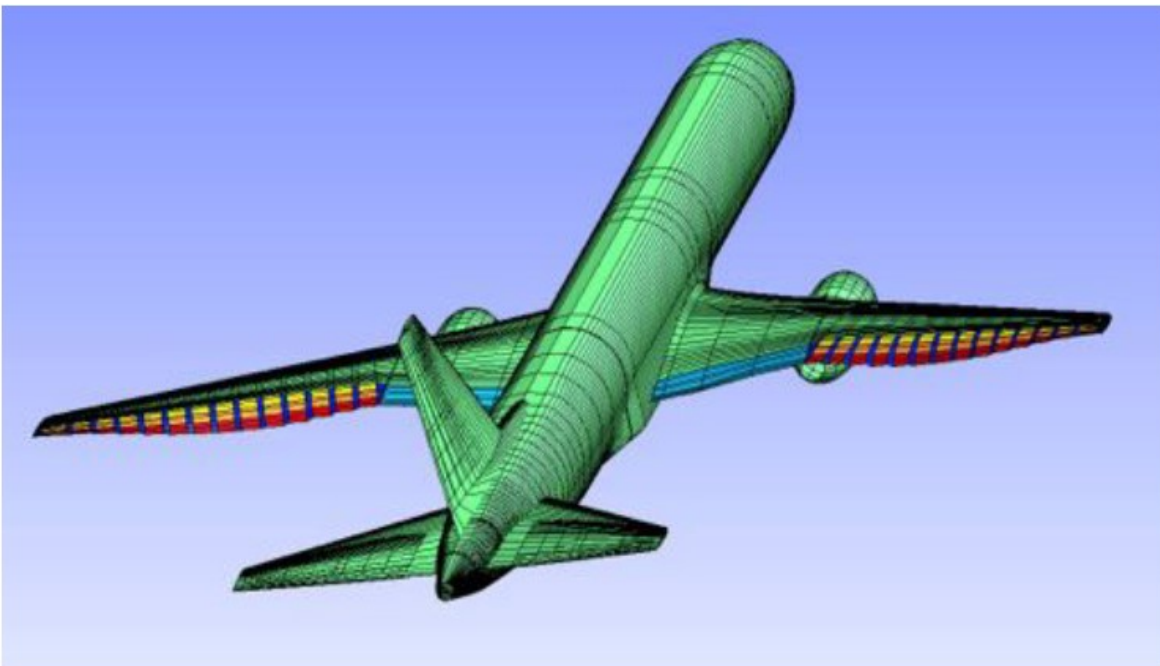

Figure 71: Full span VCCTEF GTM model [1,3]

Based on the success of the Variable Camber Continuous Trailing Edge Flexible Wing design, and the ability of FlightStream® to capture the aerodynamics gains for these configurations, more realistic bird-like wing conceptual designs are modeled in this section. The

geometry is modeled in Open VSP which has a similar planform to VCCTEF wind tunnel model with slight changes. Since this is not a validation case, there was freedom to change some dimensions from the companion wind tunnel model. This is also a semi-span model with a fuselage length of 96 inches, root and tip chord of 30.12 and 7.14 inches respectively and span of 73.29 inches. The wing is swept back at 30-degree angle and is divided into 12 sections which makes getting desired geometry easy. The same airfoil as used in the OpenVSP VCCTEF Flexible Wing model is used for this model. Also, the same 4-degree twist for wing root and 0° twist for wing tip is used on the fixed wing section.

The VCCTEF Flexible Wing model had 5 sets of flaps with each set containing 3 chambered sections of the flaps making total of 15 flaps on the model. For more realistic morphing wing design, 15 spanwise flaps, 2-inches wide with a 1-inch gap between each flap is used. This geometry has only 1 flap section in chordwise direction. Each flap is modeled in a similar way to VCCTEF model. The leading edge of the main wing was trimmed in X direction to create a space for flaps. Each flap is modeled with the MS wing component in Open VSP set at 0 sweep angle.

Since the length of the flaps are unknown, a reference wing geometry is used to get the most accurate dimensions possible. The reference wing has the exact same dimensions as the fixed wing without trailing edge trimming. Each Multi-surface wing flap is then modeled with 2inch wingspan. Its leading and trailing edge is matched with the reference wing section. To get the exact length of flap needed, the leading edge of the MS-wing component modelled as a flap is trimmed in X direction up to the point where its leading-edge match with the trimmed trailing edge of the main fixed wing geometry. A similar method is used to model all 15 flaps in Open VSP. The completed VSP model is shown in Figure 72 and 73.
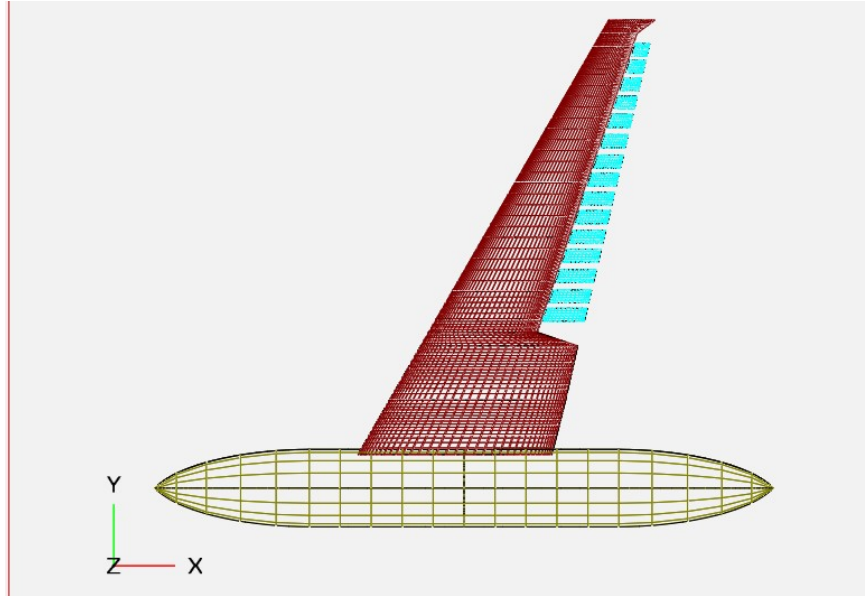
Figure 72: Morphing wing VSP model (Top view)
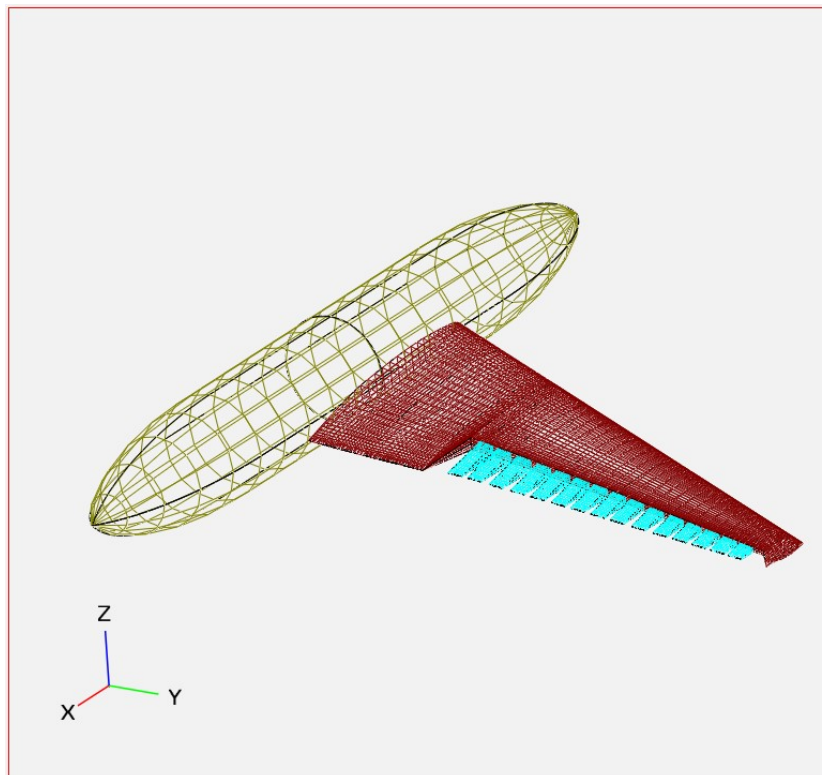
Figure 73: Morphing Wing VSP model (ISO view)

After completing the geometry, an unstructured mesh is obtained in VSP using COMPGEOM in the analysis tab. This Unstructured mesh file is then exported to FlightStream® using the .stl format for further mesh improvement as required, especially for the gaps between the tabs, and for analysis.
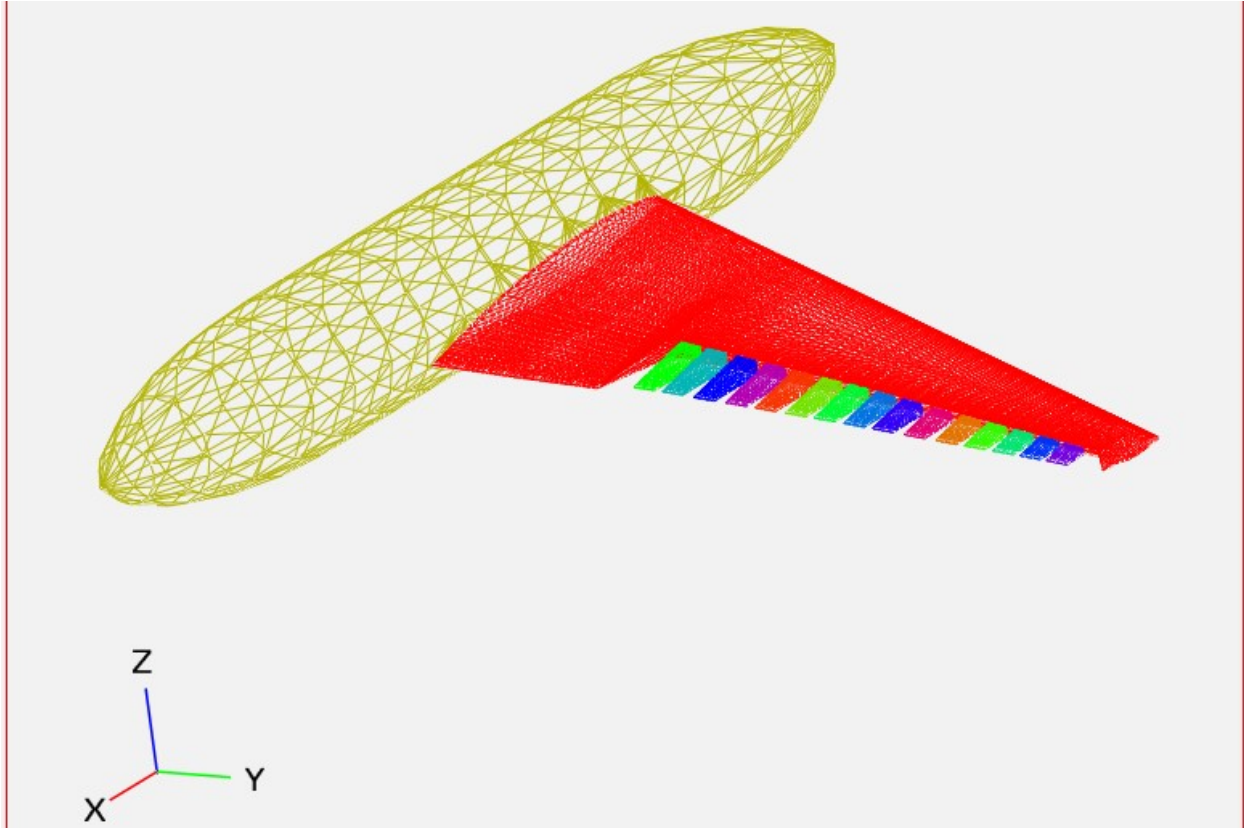
Figure 74: Unstructured mesh generated in Open VSP

5.2 FlightStream Mesh Repair:

After importing the VSP model in FlightStream®, mesh repair/completion is conducted, and the flaps are deflected to specific angle using user defined as well as reference co-ordinate system. The model is modified to obtained two different deflection cases. In one, flaps are deflected from 15 to 1 degree starting from inboard flap to outboard flap respectively. And for second case, flaps are deflected from 1 degree to 15 degree i.e. minimum to maximum deflection starting from inboard to outboard flap respectively.

The mesh repair process is similar to mesh repair completed to all VCCTEF configuration. First, the flaps are translated in Y direction so that the gap between them is 1 inch. Then user co-ordinate system is created for each flap which are 15 total and defined at the hinge

point of the flaps. The flaps are then rotated about the Y axis with the required deflection angle (15 to 1 and 1 to 15 degree) of user-defined coordinate system and about X and Z axis of reference co-ordinate system as required to match the flap's leading edge as accurately as possible with the trailing edge of the fixed wing section. After completing all the rotations, the next step is to form continuous trailing edge. This was completed in the exact same manner as in VCCTEF model, by deleting intermediate faces of the flaps and then joining the free edges of the flap with the next flap in spanwise direction. Free edges between adjacent fixed wing section and the first flap as well as fixed wing section and the last flap are also joined in spanwise direction. The completed mesh repair model is shown in Figure 77. Keep in mind that there is currently a more user-friendly solution to this meshing process available in FlightStream®
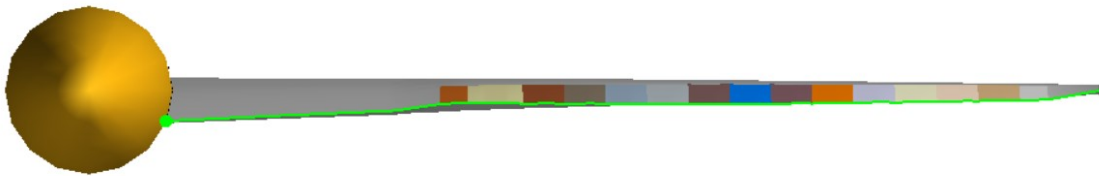
Figure 75: 1 to 15-degree deflection model (Back view)
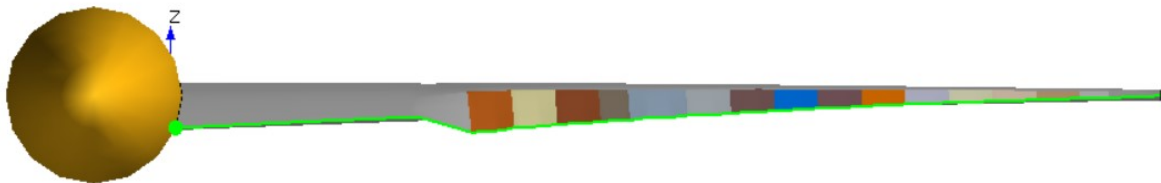
Figure 76: 15 to 1-degree deflection model (Back view)
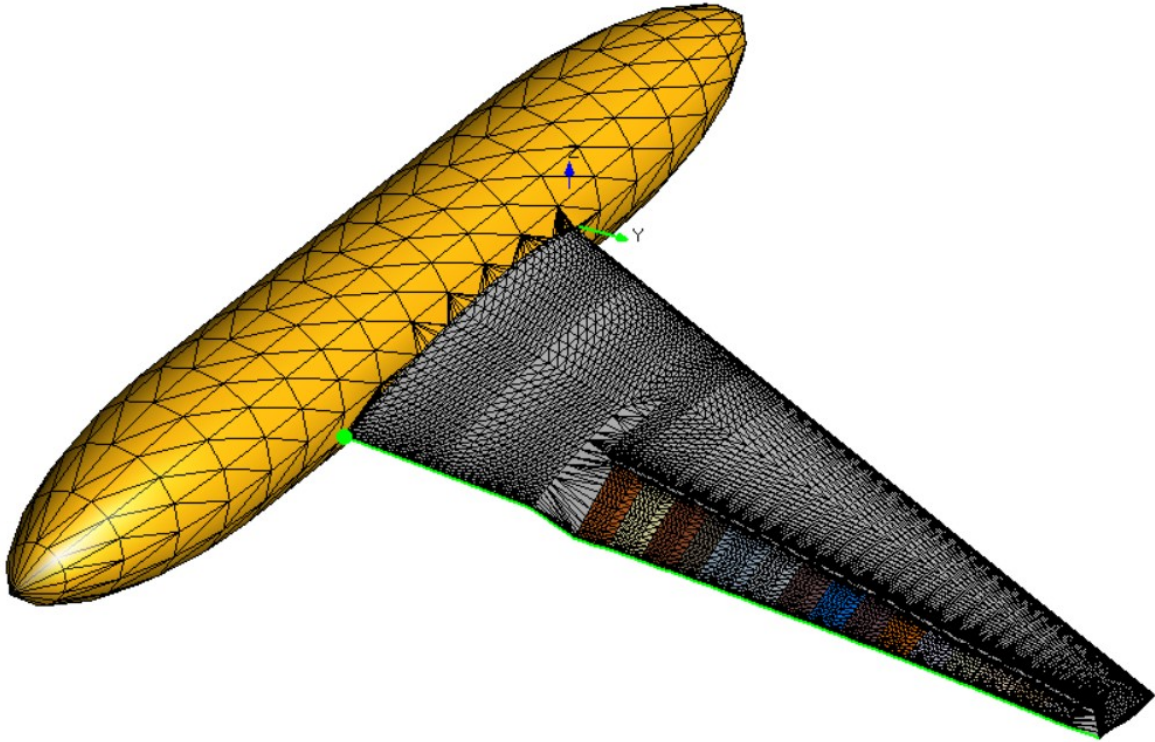
Figure 77: Model after mesh repair in FlightStream

After completing deflections and joining flaps for continuous trailing edge, the wing shaped to resemble a bird wing with the trailing edge shape close to bird scales. This is shown in figure 78 and 79 for both FlightStream® models.
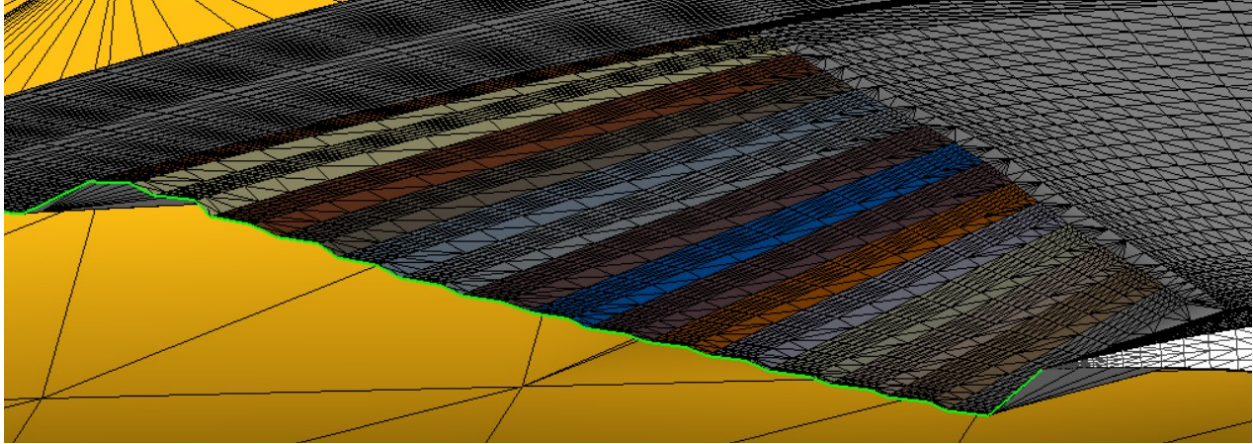
Figure 78: 1 to 15-degree flap deflection model
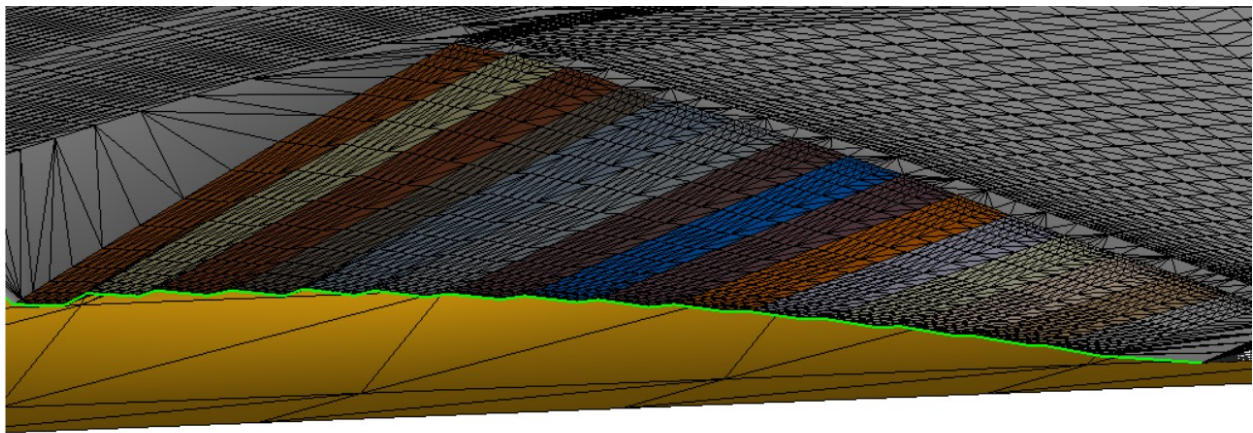
Figure 79: 15 to 1-degree flap deflection model

The green highlight on the wing represents the trailing edge. All 15 flaps and the fixed wing are marked for trailing edges and wake termination node was detected automatically before initializing the solver. Solver was run at Mach number 0.1161 at sea level conditions with reference area 0.89 m^2 and reference length of 2.95 m. The results of this simulation are shown Chapter 6.

Chapter 6

Conceptual Morphing Wing Demonstration: Results

Low-speed aerodynamic analysis is completed for both the models for angle of attack ranging from 0 to 4 degree. The vorticity model for loads and moments calculations at 0 feet altitude and 39.5 m/s speed similar to wind tunnel test is used for following results. Figure 82 and 83 shows comparison for lift curve and drag polar for both deflection models.
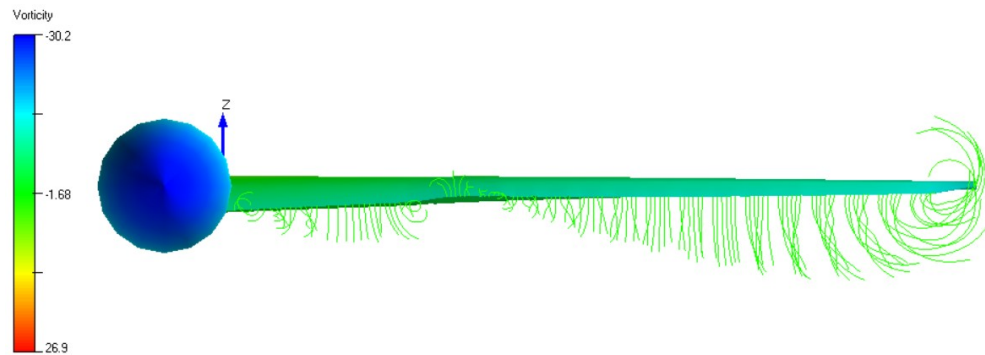
Figure 80: Vortex shedding for 1 to 15 configurations
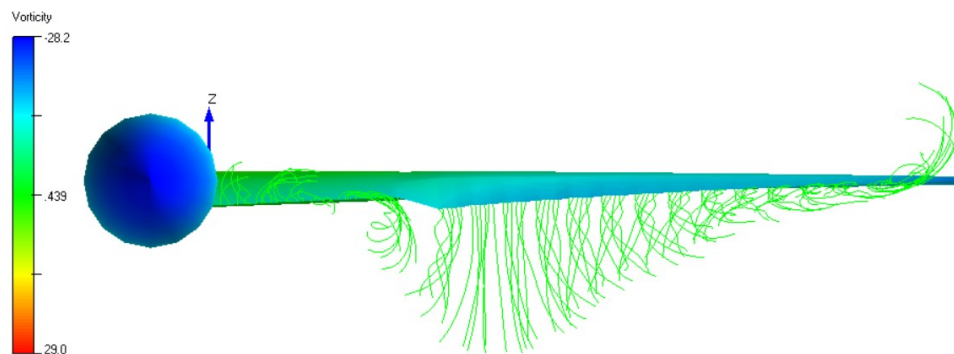
Figure 81: Vortex shedding for 15 to 1 configuration
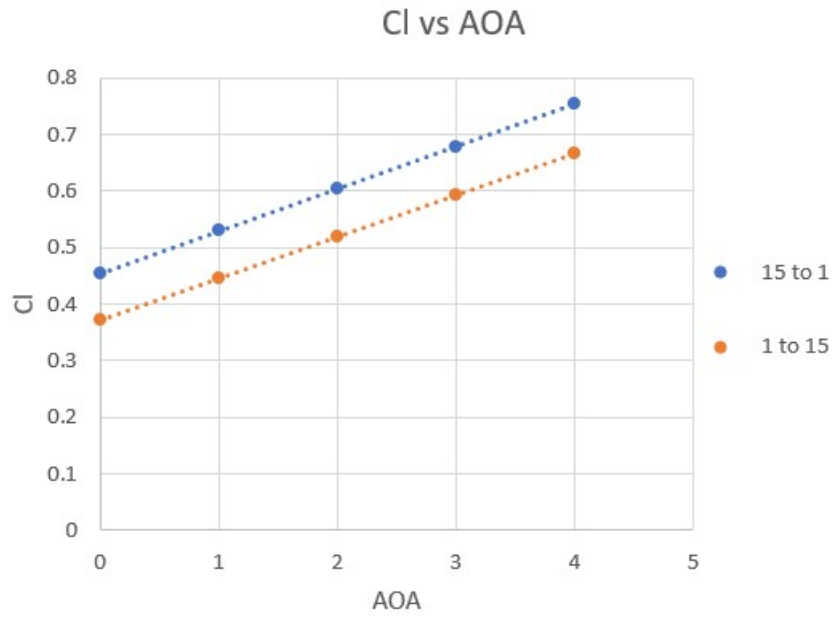
Figure 82: Lift curve comparison
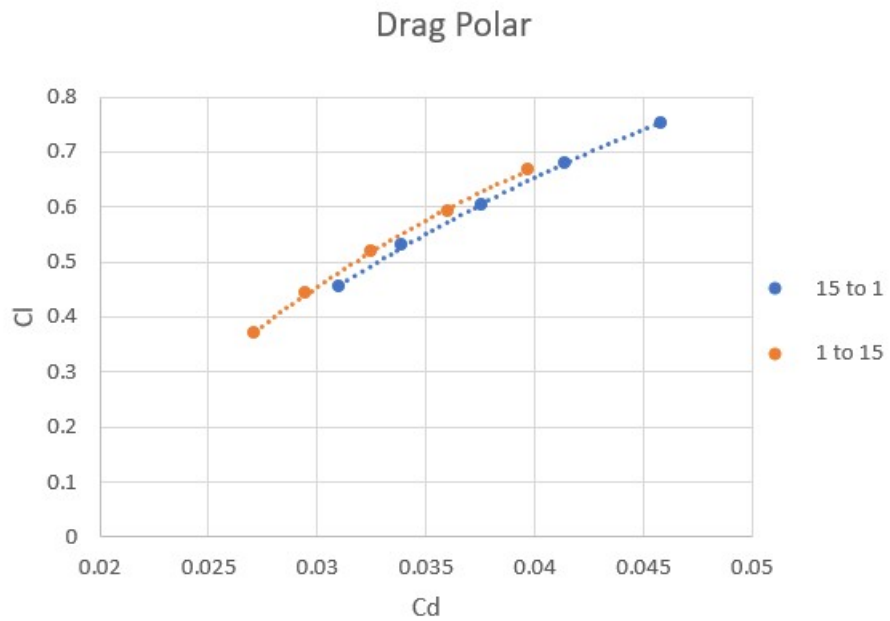
Figure 83: Drag Polar comparison
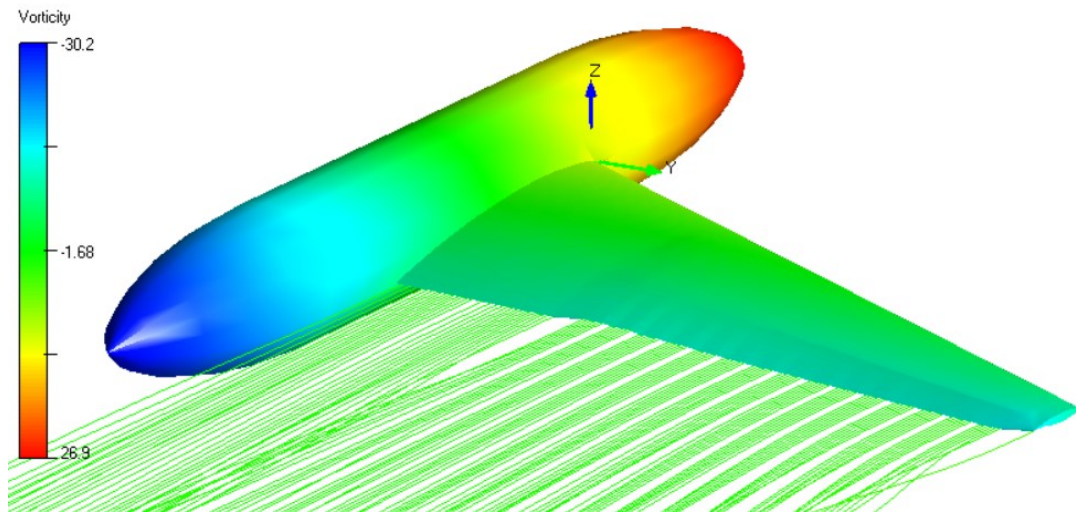
Figure 84: Vorticity distribution 1-15 configuration
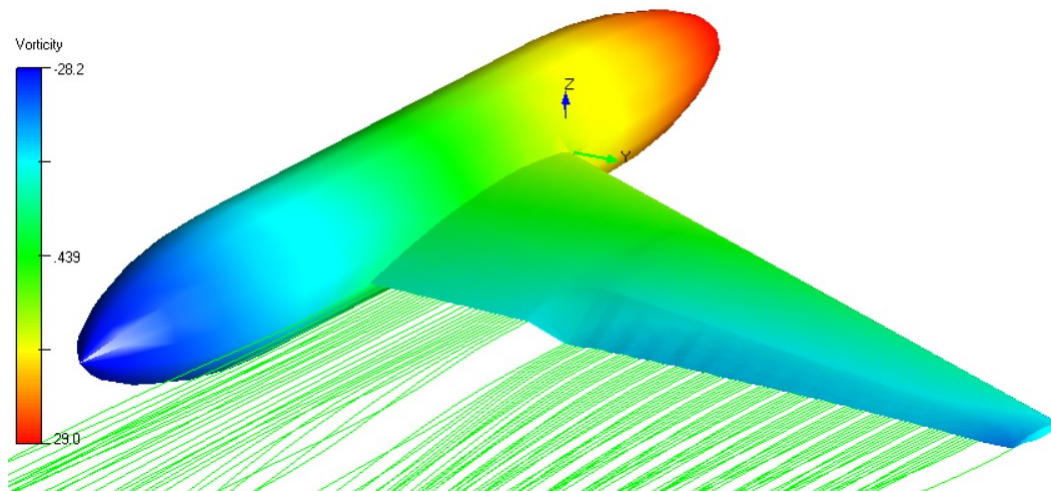
Figure 85: Vorticity distribution for 15-1 configuration

From the results presented above, it can be seen the model with deflection angle varying from 1 to 15 i.e. minimum to maximum starting from inboard to outboard flap is more aerodynamically efficient than the model with flap varying from higher to lower deflections. Cd

at ideal lift coefficient for 1-15-degree model is about 0.0320 and for 15-1-degree model is 0.0326 which is 1.85% lower than 1-15-degree configuration. Maximum L/D for 1-15 model is 16.8 which is 2.38% higher than 15-1-degree deflection model. Solution for lift, drag, vorticity and moment was conserved.

Increasing flap deflection towards the wing tip seems to be more aerodynamically efficient compared to highest deflection towards wing root. This might seem counter intuitive due to increase in spanwise load towards wing tip in 15-1 configuration, that would cause lift distribution to deviate more from the ideal elliptical lift distribution. How these configurations effect L/D, to see that we have to look at combined rigid and flexible effective angle of attack distribution along the span in each case [1]. These flaps can be deflected as per the performance requirement. Numerous possible combinations of deflections like, all flaps at maximum deflection, maximum deflection at the midspan and minimum at the inboard and outboard flaps etc. can result in aerodynamically efficient morphing wing.

Chapter 7

Conclusion and Future work

Based on the results obtained in the validation case and the conceptual morphing wing demonstration, FlightStream® proved to be reliable in predicting the aerodynamic characteristics of morphing wings. The concept of morphing wing was introduced in order to decrease the drag and fuel consumption and hence increasing the efficiency of the aircraft at the cruise. This FlightStream® based analysis demonstrated that a vorticity method such as FlightStream® can be used to determine the most beneficial configuration for drag minimization relative to a baseline (FLAP0) case. In validation cases, drag reduction and L/D max percent difference between FlightStream® and wind tunnel results is within 5% for majority of cases. Overall the results prove that FlightStream® is capable of capturing morphing wing trends to the excellent level of accuracy. The viscous component of the results obtained for C_d and L/D will vary with aircraft scale, but this effect can be captured by FlightStream®. The presence of the vertical stabilizer and the horizontal tail, the engines and high-speed flight are expected to affect the performance of VCCTEF so no generalization about morphing wings more broadly is being asserted.

To more accurately assess the advantages of morphing wings aerodynamically, the demonstration geometry results should be compared with the baseline model with all the flaps at 0° deflection. This analysis will be completed in the future to assess more fully the drag reduction benefits of the conceptual refined morphing wing design.

Several Aerospace engineers are working on developing morphing wing technology including designs that can bend and flex like the wings of bats and birds covered with the skin

of overlapping faces which resemble feathers or scales. Different types of wing morphing include variable camber, variable span and variable sweep. NASA and MIT's new morphing aircraft design is made of mechanical "Metamaterial" consisting of thousands of tiny polymer tiles which resemble a method of "building block". Some modules in this structure are rigid and some are flexible. Rigidity and flexibility of each module influence how a wing flexes when force is applied to it. Another approach to achieve wing morphing is a use of piezoelectric materials which use electricity to affect physical movement coupled with shape memory alloy that can change shape with the application of an electric potential. [20]

Morphing technology is not just limited to aircraft wings. This concept can be extended to the entire aircraft whose shape can be deformed for aerodynamic advantage. This idea extends even beyond aviation to biological and energy systems. There is a possibility of having wind turbines driven by giant morphing rotors that collect wind energy in more efficient way. This concept might inspire a robotic body, with arms and legs which can change shape and bend continuously across their entire length instead of only at fixed joints. One day we could possibly have boats or submarines that behave more like fish.[20]

Morphing technology appears to figure prominently in the future of aviation . After seeing remarkable results of morphing wing in subsonic flight, curiosity is how it will affect the performance of supersonic flights? To explore this question, reliable and validated aerodynamic analysis tools are required. This thesis presents one small step in the long effort to provide these tools.

Reference

1) "*Experimental Investigation of a Flexible wing With Variable Camber Continuous Trailing Edge Flap Design*", Nhan Nguyen ,NASA Ames Research Center, Moffett Field, CA 94035,Nathan Precup, University of Washington, Seattle, WA 98195,James Urnes, Sr. Boeing Research & Technology, St. Louis, MO 63134,Chester Nelson, Boeing Commercial Airplanes, WASonia Lebofsky , Stinger Ghaffarian Technologies Inc., Moffett Field, CA 94035, Eric Ting k, Stinger Ghaffarian Technologies Inc., Moffett Field, CA 94035, Eli Livne, University of Washington, Seattle, WA 9819.

2) "*Elastically Shaped Wing Optimization and Aircraft Concept For Improved Cruise Efficiency*", Nhan Nguyen, NASA Ames Research Center, Moffett Field, CA 94035 Khanh Trinh t, Stinger Ghaffarian Technologies Inc., Moffett Field, CA 94035,Kevin Reynolds, NASA Ames Research Center, Moffett Field, CA 94035, James Kless, Science & Technology Corp. , Moffett Field, CA 94035,Michael Aftosmis'll, NASA Ames Research Center, Moffett Field, CA 94035,James Urnes, Sr.11,Boeing Research & Technology, St. Louis, MO 63166,Corey Ippolito,NASA Ames Research Center, Moffett Field, CA 94035

3) "*Aeroelastic Analysis of Flexible wing Wind tunnel Model with Variable Camber Continuous Trailing Edge Flap Design*", Nhan Nguyen, NASA Ames Research Center, Moffett Field, CA 94035,Eric Ting Stinger Ghaffarian Technologies Inc., Moffett Field, CA 94035, Sonia Lebofsky, Stinger Ghaffarian Technologies Inc., Moffett Field, CA 94035

4) "*Development of variable Camber continuous Trailing Edge Flap for Performance Adaptive Aeroelastic Wing*", Nhan Nguyen, Upender Kaul, NASA Ames Research Center, Moffett Field, CA 94035, Sonia Lebofsky, Eric Ting, Daniel Chaparro,Stinger Ghaffarian Technologies, Inc.,NASA Ames Research Center, Moffett Field, CA 94035, James Urnes, Boeing Research and Technology, St. Louis, MO 63134

5) " *Aerodynamic Loads Over Arbitrary Bodies by method of Integrated Circulation*", Vivek Ahuja, Auburn University, 2013

6) "*Aircraft High Lift Aerodynamic Analysis using Surface Vorticity Solver*", Eric D. Olson and Cindy W. Alberton, 55th AIAA Aerospace Science Meeting, San Diego, CA

7) " *Three- Dimensional Modelling of Aircraft High-Lift Components with Vehicle Sketch Pad*", Eric D. Olson, 54th AIAA Aerospace Sciences Meeting 2016, San Diego, CA.

8) " *Design and Construction of a Wind Tunnel Model with Active Variable Camber Continuous Trailing Edge Flap for Aeroelastic "In-Flight" Shape Optimization Tests*", Nathan Precup, University of Washington, 2018

9) "*Examination of Flightstream for Proximity Flight with stores*", Eric Mathew Todd, Auburn University 2017

10) " *Aerodynamic Optimization of Integrated Wing-Engine Geometry Using an Unstructured Vorticity Solver*", Logan King, Auburn University, 2015

11) " *Morphing Wing: A demonstration of Aero Servo Elastic Distributed Sensing and Control*", Sunil C. Patel, AIAA 2005.

12) " *Morphing Aircraft Technology- New Shapes for Aircraft design*", Terrence A. Weisshaar, Department of Aeronautics and Astronautics, Perdue University, 2006

13) http://openvsp.org/wiki/doku.php?id=files

14) " *Morphing Wings are First step toward bird like Aircraft*", Charles Q. Choi, Live Science, 2016.

15) " *Fundamentals of Aerodynamics",* John D. Anderson

16) *" Theory of Wing Sections",* Ira H. Abbott

17) http://openvsp.org/wiki/doku.php?id=tutcompgeom

18) *"Flightstream User Manual"*

19) http://www.aerospaceweb.org/question/airfoils/q0073.shtml

20) *" A 100-year-old idea that could change flight",* Charles Choi, Nova Next, 2017

21) "*INVESTIGATING THE BENEFITS OF MORPHING WING TIP DEVICES - A CASE STUDY*", Chen Wang , Hamed Haddad Khodaparast , Michael I Friswell, IFASD 2015.

22) *"Low speed aerodynamics: from wing theory to panel method",* Katz, J. and Plotkin, McGraw-Hill Inc. ISB-0-07-050446-6,1991

23) *"Aero-Propulsive Analysis for Contemporary Conceptual Design",* Vivek Ahuja, Imon Chakraborty, Roy Hartfield, Aviation conference 2019.

Appendix A

DEMO GEOM AIRFOIL FILE

GTM

0   Sym Flag (0 - No, 1 - Yes)

12   Num Pnts Upper

17   Num Pnts Lower

0	0
0.017961571	0.011695906
0.041353383	0.018796992
0.058897243	0.02213868
0.135338346	0.033834586
0.249791145	0.046783626
0.35380117	0.051796157
0.550543024	0.051796157
0.657059315	0.04887218
0.769423559	0.036340852
0.918128655	0.011695906
1	-0.004177109

0	0
0.00459482	-0.008354219
0.031328321	-0.014619883
0.064745196	-0.018379282
0.099415205	-0.022556391
0.142857143	-0.027986633
0.183792815	-0.032999165
0.241854637	-0.03968254
0.304511278	-0.046365915
0.413533835	-0.046365915
0.499582289	-0.043859649
0.557226399	-0.03968254
0.676691729	-0.018379282
0.714703425	-0.012531328
0.817042607	-0.006683375
0.908103592	-0.004177109
1	-0.004177109

Appendix B

FlightStream results for Validation Case using Vorticity Loads and Moments model:

FLAP0:

AOA	C_l	C_d
0	0.1828	0.0193
1	0.2485	0.0208
2	0.3144	0.0228
3	0.3801	0.0254
4	0.4458	0.0284
5	0.5114	0.0319
6	0.5769	0.0358

FLAP1:

AOA	C_l	C_d
0	0.3895	0.0263
1	0.4545	0.0292
1.5	0.4867	0.0308
2	0.5191	0.0327
2.5	0.5514	0.0347
3	0.5838	0.0367

FLAP2

AOA	C_l	C_d
0	0.3307	0.0237
1	0.3958	0.0261
2	0.4613	0.0293
3	0.5262	0.0329
4	0.5914	0.0368

FLAP3

AOA	C_l	C_d
1	0.3918	0.0256
2	0.4572	0.0285
3	0.5225	0.0321
4	0.5876	0.036

FLAP4:

AOA	C_l	C_d
0	0.2873	0.0217
1	0.3526	0.0239
2	0.4179	0.0267
3	0.4831	0.03
4	0.5483	0.0337
4.5	0.5813	0.0356

FLAP5:

AOA	C_l	C_d
1	0.3428	0.0241
2	0.4082	0.0266
3	0.4736	0.0299
4	0.5386	0.0335
4.5	0.5713	0.0355

FLAP6:

AOA	C_l	C_d
0	0.2108	0.0197
1	0.2763	0.0214
2	0.3419	0.0236
3	0.4074	0.0264
4	0.4728	0.0295
5	0.5382	0.0332

	6	0.5707	0.035

FLAP7:

AOA	C_l	C_d
1	0.2937	0.0218
2	0.359	0.0241
3	0.4244	0.0269
4	0.4897	0.0303
5	0.5549	0.034

FLAP8

AOA	C_l	C_d
0	0.2087	0.0196
1	0.2741	0.0212
2	0.3397	0.0234
3	0.4051	0.026
4	0.4706	0.0293
5	0.5359	0.033

FLAP9

AOA	C_l	C_d
0	0.2784	0.0211
1	0.3445	0.0233
2	0.41	0.0259
3	0.4753	0.0292
4	0.5405	0.0327
5	0.6057	0.037

FLAP10

AOA	C_l	C_d
0	0.2533	0.0204

1	0.3188	0.0223
2	0.3843	0.0249
3	0.4497	0.028
4	0.5151	0.0313
5	0.5804	0.0354

FLAP11

AOA	C_l	C_d
0	0.1212	0.0193
1	0.1875	0.0203
2	0.2532	0.0218
3	0.3188	0.0239
4	0.3844	0.0262
5	0.4498	0.0294
6	0.5152	0.0329